

Characterization and validation of novel anti-CB1 monoclonal
antibodies and their application to GPCR studies

By

Triona Matheson

A Thesis

Presented to the Department of Biochemistry and Molecular Biology
at Oregon Health and Science University
School of Medicine

In partial fulfillment of requirements

For the degree of:

Masters of Science in Biochemistry and Molecular Biology

October, 2024

Table of Contents

List of Figures	iii
List of Tables	vi
List of Abbreviations	vii
Acknowledgements	xi
Abstract	xii
Chapter 1: Introduction	1
1.1 GPCR Overview	1
1.2 CB1 General Background	2
1.3 CB1 Expression and Signaling	2
1.4 CB1 N-terminal Background	3
1.5 Anti-CB1 Antibodies	5
1.6 Overview of Thesis	6
1.7 Figures	7
Chapter 2	12
2.1 Introduction	12
2.2 Methods	13
2.3 Results	16
2.4 Discussion	19
2.5 Future directions	21
2.6 Figures	21
2.7 Tables	32
Chapter 3	36
3.1 Introduction	36

3.2 Methods	37
3.3 Results	39
3.4 Discussion	41
3.5 Figures	43
3.6 Table	50
Chapter 4	51
4.1 Introduction	51
4.2 Methods	53
4.3 Results	55
4.4 Discussion	57
4.5 Results	59
4.6 Table	66
Chapter 5: Summary and Future Directions	67
5.1 Summary of Significance	67
5.2 Characterization and validation of novel anti-CB1 antibodies	68
5.3 Role of the CB1 N-terminus in CB1 subcellular localization	69
5.4 Affinity-based purification strategies	70
References	72
Appendix 1: Primer list	78
Appendix 2: Edman sequencing of proteolytic product of CB1	80
Appendix 3: Live cell confocal microscopy of glycosylation-deficient mutant CB1	82

List of Figures

Figure 1.1: Schematic of GPCR structure	8
Figure 1.2: Schematic of CB1 signaling and internalization	9
Figure 1.3: Sequence logos describing the different splice variants of mammalian CB1N-termini detected in a multiple-sequence analysis (MSA)	10
Figure 1.4: The CB1 N-terminus is predicted to undergo proteolytic cleavage and glycosylation	10
Figure 1.5: Cysteine residues in the membrane proximal region (MPR) of the CB1 N-terminus can modulate receptor-ligand interactions	11
Figure 2.1: Schematic of CB1 with relevant regions highlighted and slot blot of various CB1 mutants imaged with anti-CB1 antibodies as indicated	21
Figure 2.2A: Peptide competition IP of 3A3 and 5G3 with quantitation	22
Figure 2.2B: IL3 deletion mutant western blots	23
Figure 2.2C: Double alanine scan of IL3	24
Figure 2.2D: Double alanine scan of IL3	24
Figure 2.3A: Peptide competition of immunoprecipitation of CB1_GL with 1E10	25
Figure 2.3B: Peptide competition of immunoprecipitation of CB1_GL or CB1_GL_G88 at various peptide concentrations	25
Figure 2.3C: Dual alanine scan of CB1_GL mutants map the requirements of the 1E10 epitope	26
Figure 2.3D: Single alanine scan of CB1-GL mutants identify key residues in the 1E10 epitope	26

Figure 2.4A: Peptide competition studies indicate N-terminal acetylation is needed for the 1E10 epitope peptides to compete with 1E10 binding	27
Figure 2.4B: Peptide competition immunoprecipitation with CB1_GL with 1E10 and short peptides with methionine	27
Figure 2.5A: Immunofluorescence of CB1_GL with 1E10	28
Figure 2.5B: Immunofluorescence of CB1_GL with 3A3	28
Figure 2.5C: Immunofluorescence of CB1_GL with 5G3	28
Figure 2.6A: Schematic of 10- and 4- residue additions corresponding to the 1E10 epitope to the N-terminus of rhodopsin	29
Figure 2.6B: 10- and 4- residue tags for visualization with 1E10	29
Figure 2.6C: Difference spectra of shRho and tagged-shRho mutants	30
Figure 2.6D: Immunofluorescence of transient transfection of 4- residue addition mutant rhodopsin or shRho stained with 1E10 or 1D4	31
Figure 3.1A: Various concentrations of TransfeX and DNA were tested in the transfection of SFKE_CB1_C2 in HEK 293 cells	43
Figure 3.1B: Various concentrations of large T-antigen plasmid were tested in the transfection of both HEK 293 cells with SFKE_CB1_C2	44
Figure 3.2A: Schematic of multiplexed immunofluorescence with fluorescently conjugated Fabs	45
Figure 3.2B: Validation of immunofluorescent staining with fluorescently labeled anti mouse antibody Fab	45
Figure 3.3: Confocal images of HEK cells transiently transfected with SFKE_CB1_C2	46

Figure 3.4A: Immunofluorescence of CB1 N-terminal truncation mutant, GL	46
Figure 3.4B: Immunofluorescence of tagged, full-length receptor, SFKE_CB1_C2	47
Figure 3.5: Live cell staining of surface receptor	47
Figure 3.6A: Immunofluorescence of shCB1_C2 with colocalization analysis	48
Figure 3.6B: Immunofluorescence of shCB1_C2 N77Q, N83Q with colocalization analysis	49
Figure 4.1: Purification of CB1_GL with 1E10 and 1D4 in RIPA	59
Figure 4.2: Purification of CB1_GL with 1E10 in PBSSC + 1% DDM	60
Figure 4.3A: Mutations in the N-terminus of CB1_GL decrease the affinity of 1E10 for the receptor	60
Figure 4.3B: Purification of CB1 GL N-terminal mutants with 1E10 or 1D4	61
Figure 4.3C: Immunoaffinity purification of CB1_GL with 1E10 with PBSSC + DDM	61
Figure 4.4A: Purification of tagged rhodopsin mutants with 1E10 or 1D4.	63
Figure 4.4B: Large-scale purification of tagged rhodopsin	64
Figure 4.5A: Multivalent 1D4 peptide for improved elution from 1D4 column	64
Figure 4.5B: Test of multivalent SFKE peptide for improving elution from 1E10 column	65
Figure A2: Coomassie stained PVDF membrane from SDS-PAGE of CB1_NtG9	81
Figure A3: Immunofluorescence and western blot of shCB1_C2 or shCB1_C2 N77Q/N83Q in HEK 293 GNTI-	83

List of Tables

Table 2.1: CB1 Monoclonal Antibody concentrations and remaining aliquots at -80 C	32
Table 2.2: Phusion PCR	32
Table 2.2A: PCR set-up	32
Table 2.2B: PCR cycling conditions	33
Table 2.3: Overlap extension PCR Step 1	33
Table 2.3A: PCR set-up	33
Table 2.3B: PCR Cycling conditions	34
Table 2.4: Overlap extension PCR step 2	34
Table 2.4A: PCR set-up	34
Table 2.4B: PCR cycling conditions	35
Table 2.5: Peptides used in immunoprecipitation studies	35
Table 3.1: Colocalization analysis summary for shCB1_C2	50
Table 3.2: Colocalization analysis summary for shCB1_C2 N77Q, N83Q	50
Table 4.1: Peptides obtained from Genscript for use in protein purification.	66
Table A1: Primer list and primer properties.	78

List of Abbreviations

Abbreviation	Meaning
1D4	Mouse monoclonal anti-rhodopsin antibody. Specifically binds to the C-terminal epitope TETSQVAPA-COOH of rhodopsin.
1E10	Mouse monoclonal anti-CB1 antibody. Specifically binds to an N-terminal eptope SFKENEENIQ with N-terminal acetylation.
1E10-Rho	sythetic human rhodopsin mutant with 10-residue (SKENEENIQ) addition N-terminally
2-AG	2-Arachidonoylglycerol
3A3	Mouse monoclonal anti-CB1 antibody. Binds an epitope in the intracellular loop 3 region of CB1
5G3	Mouse monoclonal anti-CB1 antibody. Binds an epitope in the intracellular loop 3 region of CB1
A	alanine
Ab	antibody
AEA	Anandamide/N-arachidonoylethanolamine
BPB	bromophenol blue
C	cysteine
°C	degrees celcius
Ca+	calcium cation
CB1	cannabinoid type 1 receptor
CB1a	cannabinoid type 1 receptor isoform a
CB1b	cannabinoid type 1 receptor isoform b
CB1-GL	N- and C-terminal truncation ($\Delta 87$ and $\Delta 417$) mutant of shCB1-C2

CB1- Δ IL3	is a modified shCB1-C2 with an N-terminal truncation (Δ 87 like GL) with IL3 deleted
CIP	cow intestinal phosphatase
CNR1	gene encoding the cannabinoid type 1 receptor and splice variants
COS-1	cell line derived from monkey kidney
D	aspartate
DAPI	4',6-diamidino-2-phenylindole, fluorescent nuclear stain
DMM	n-Dodecyl- β -D-Maltoside
DNA	Deoxyribonucleic acid
DTT	Dithiothreitol
E	glutamate
ECL	extracellular loop
EDTA	Ethylenediaminetetraacetic acid
F	phenylalanine
Fab	Fragment antigen-binding
FDA	Federal Drug Administration?
G	glycine
GNTI	N-acetylglucosaminyltransferase I
GPCR	G-protein coupled receptor
H	histidine
HEK 293	human embryonic kidney cell line
I	isoleucine
ICL	intracellular loop
Ig	immunoglobulin
IL3	Intracellular loop 3

K	lysine
K+	potassium cation
kDa	kilodalton
M	molar
M (residue)	methionine
mA	milliamps
MES	2-(N-morpholino)ethanesulfonic acid
mL	milliliter
mM	millimolar
MPR	membrane-proximal region
MSA	multiple sequence alignment
N	asparagine
NEB	New England Biolabs
Neuro2a	neuroblastoma cell line originating from mice
ng	nanograms
Nt	N-terminus
Nt Alo	rabbit anti-CB1 N-terminal polyclonal antibody from Alomone Labs
Nt Cay	rabbit anti-CB1 N-terminal polyclonal antibody from Cayman Chemical
OHSU	Oregon Health & Science University
P	proline
PAGE	polyacrylamide gel electrophoresis
PBSSC	phosphate buffered saline
PCR	polymerase chain reaction
PEI	Polyethyleneimine

PMSF	phenylmethanesulfonyl fluoride
PVDF	polyvinylidene difluoride
Q	glutamine
RIPA	a lysis and extraction buffer
ROI	Region of interest
S	serine
SDS	Sodium dodecyl sulfate
SFKE-Rho	synthetic human rhodopsin mutant with 4-residue addition N-terminally
shCB1-C2	full-length synthetic human CB1 with only two cysteine residues (C257 and C264) which form a disulfide
shRho	synthetic human rhodopsin mutant
T	threonine
THC	delta-9-tetrahydrocannabinol
TM	transmembrane
Tris	2-Amino-2-hydroxymethyl-propane-1,3-diol
V	volts
V (residue)	valine
VGTI	Vaccine and Gene Therapy Institute
WT	wild-type
μg	microgram
μL	microliter
μM	micromolar

Acknowledgements

I would first like to thank my mentor, Dr. David Farrens, for his guidance and wisdom. I would also like to thank my thesis advisory committee, Dr. Show-Ling Shyng, Dr. Ujwal Shinde, and Dr. Jonathan Pruneda. I would also like to thank Dr. Monica Hinds for her support. I would like to acknowledge and thank current Farrens lab member, Weekie Yao, as well as former lab members Dr. Anthony Shumate and Dr. Emily Platt for their companionship and guidance. I would also like to acknowledge former Farrens lab member Dr. Jon Fay who initially generated and characterized the antibodies that are the focus of this work.

Thank you to my PMCB 2019 cohort for their friendship and support and to the past and current members of the Graduate Researchers United Executive board for all their hard work to make graduate research the best it can be. I have loved getting to know and work with each of you.

I would also like to thank my amazing family. Thank you for your unconditional love and support through all the ups and downs over the years. You have each shaped me into the person I am today, and I am forever grateful to have you on my team. Mom and Dad, you taught me to work hard and dream big (“Do and Hope”) and never stop learning. Gregor, you have shown me the meaning of strength and the importance of kindness. You are my hero and my best friend. To my grandmothers, who are the strongest women I have ever met, thank you for showing me the importance of passion. To my grandfather, thank you for teaching me to slow down and appreciate life and for encouraging my curiosity for the world around me.

Finally, to Cesar, my incredible partner: I could not have done this without you. You and our cat, Waffles, were with me every step of the way (even when you were far away). You are my rock and my harbor in the storm. I love you and I am so proud of you.

Abstract

G-protein coupled receptors (GPCRs) are important signal transducing proteins and the target of many drugs. One example is the cannabinoid type 1 receptor (CB1), which is highly expressed throughout the central nervous system and is involved in synaptic plasticity. CB1 has an unusually long N-terminal region for a GPCR of its class, but the function of this region remains unclear. This has been a difficult question to answer as most commercially available antibodies against CB1 are polyclonal antibodies recognizing N-terminal epitopes, as polyclonal antibodies can be less reproducible and the CB1 N-terminus may be modified or proteolyzed. In this thesis, I detail the characterization and validation of several novel monoclonal anti-CB1 antibodies as well as several applications of these antibodies.

In Chapter 2, I characterized several novel anti-CB1 monoclonal antibodies and validated them for use in immunoblot, immunoprecipitation, and immunofluorescence. Of note, one of these antibodies, 1E10, binds an N-terminal epitope of a CB1 truncation mutant that has been N-terminally acetylated. I also generated and validated a 10- and 4-residue tag for use with 1E10. In Chapter 3, I used these antibodies to validate several staining techniques for use in immunofluorescent confocal microscopy. This included validation of a technique for multiplexed antibody staining with antibodies from the same source species. In Chapter 4, I demonstrated the ability of 1E10 to purify CB1 and a tagged rhodopsin. Altogether, this thesis presents novel tools and techniques to address lingering questions in the study of CB1.

Chapter 1: Introduction

1.1 GPCR Overview

G-protein coupled receptors (GPCRs) are the largest family of transmembrane proteins in the human genome, where they play key roles in signal transduction across biological membranes. They are named for the intracellular, membrane-associated proteins they interact with, G-proteins. G-proteins are heterotrimeric complexes containing alpha, beta, and gamma subunits. Upon activation, G-protein alpha subunits activate signaling proteins by hydrolyzing GTP. Activated GPCRs can bind to and activate G proteins by inducing the exchange of GDP for GTP, thus re-setting the G-protein ¹.

In addition to G-proteins, GPCRs can interact with several other intracellular proteins. Conformational changes involved in GPCR activation allow the intracellular region of the receptor to be phosphorylated by G-protein-coupled receptor kinases (GRKs) ². For many GPCRs, this phosphorylation promotes interaction between GPCRs and arrestins, which induce clathrin-mediated endocytosis of receptors ^{2,3}. Once internalized, the GPCRs can be recycled to the surface or targeted for degradation in the lysosome ³.

Structurally, GPCRs consist of seven transmembrane alpha helices with an N-terminal region on the extracellular side of the membrane and the C-terminal region on the intracellular side of the membrane (Figure 1.1). GPCRs interact with a variety of ligands and modulatory proteins. GPCR ligands vary widely and include lipids, peptides, hormones, and numerous other small molecules ⁴. Their important role in signal transduction makes this class of proteins highly druggable. In fact, 30-40% of all FDA approved drugs in 2016 targeted a GPCR. Most of these drugs target a class A, or rhodopsin-like, GPCR, which are the largest class of GPCRs ⁵. This class is named for rhodopsin, a visual photoreceptor responsible for dim light vision. Rhodopsin has been a model system for studying GPCRs, and the first structure of a GPCR was of rhodopsin ⁶. Class A GPCRs generally have short N-terminal regions which can be modified post-translationally in several ways including glycosylation and proteolysis ⁷. The work in this

thesis primarily focuses on one class A GPCR, the cannabinoid type 1 receptor (CB1). Rhodopsin studies are also included for comparison because, as noted above, it is a classical and well-studied GPCR.

1.2 CB1 General background

Interest in CB1 initially arose because it is activated by delta-9-tetrahydrocannabinol (THC), the primary psychoactive agent of *Cannabis sativa*⁸. Subsequently, an endocannabinoid system was discovered that includes endogenous CB1 ligands N-arachidonylethanolamine (Anandamide) and 2-Arachidonoylglycerol (2-AG)⁹⁻¹¹. Alterations in the endocannabinoid system have been implicated in several disease states including Parkinson's disease, Alzheimer's disease, multiple sclerosis, epilepsy, depression, and more^{12,13}.

CB1 is encoded by the gene CNR1, which has three known splice variants that result in translation of three unique CB1 isoforms. Interestingly, these isoforms only vary in the first 88 residues of the N-terminal domain. Full length CB1 (herein referred to as CB1) is the most studied and longest isoform. Compared to CB1, variant CB1a contains a shorter and dissimilar N-terminus while CB1b lacks residues 22 - 54 of CB1¹⁴.

CB1a and CB1b have been found throughout the central nervous system and peripheral tissue. Although they show lower level of transcripts than CB1¹⁴⁻¹⁷, these isoforms may be expressed more efficiently due to their shorter N-terminal regions. *In vitro* studies show both CB1a and CB1b, and CB1 N-terminal truncation mutants often exhibit increased expression in cell culture¹⁸. This work will focus on the first variant, CB1, and mutants of CB1.

1.3 CB1 Expression and signaling

CB1 is also highly expressed throughout the central nervous system, where it is involved in a variety of processes including modulation of neurotransmitter release in neurons. CB1 is typically located

primarily at the pre-synapse, where it is involved in synaptic plasticity and resetting of the synapse ^{19–25}. CB1 is activated by endocannabinoids that are produced in the post-synapse in response to post-synaptic receptor activation by neurotransmitters released by the pre-synaptic cell. In this way, CB1 acts to reset signaling between pre- and post- synaptic neurons. CB1 activation of G-proteins G_i and/or G_o can reduce voltage gated calcium current amplitudes ²⁶, modify voltage-sensitive potassium current (I_A) ²⁷, and reduce intracellular cAMP ²⁸, Figure 1.2.

Like many GPCRs, internalization and recycling of CB1 can also occur once activated. As shown in Figure 1.2, binding of beta-arrestin recruits internalization factors and results in the formation of endosomes containing activated receptors. These receptors can then be recycled to the plasma membrane or targeted for degradation ²⁸.

There is also increasing evidence for an intracellular population of CB1. Of note for this thesis, this localization is thought to involve the first 22 N-terminal residues of CB1, which have been proposed to act as a mitochondrial targeting sequence ²⁹. This intracellular, mitochondrial population has been shown to regulate neuronal metabolism ^{30,31}. While this presents a role for the N-terminus in mitochondrial targeting, it remains unclear how surface expression of the receptor is regulated.

1.4 CB1 N-terminal background

Intriguingly, the CB1 N-terminus is unusually long (~ 116 residues), one of the longest N-termini for a Class A GPCR ³². This is puzzling for a receptor that is thought to bind hydrophobic ligands through membrane-embedded transmembrane helices ^{33,34}. Moreover, most of the N-terminal residues are not needed for binding synthetic orthosteric ligands – the first 103 residues can be deleted with little apparent effect on synthetic ligand binding ³⁵.

To see if a long CB1 N-terminus is a conserved feature, Dr. Ujwal Shinde (OHSU, unpublished) carried out an extensive bioinformatics analysis of 638 sequences from CB1 eukaryotic homologs in the

UniProtKB and Swiss-prot database (Figure 1.3). The results were surprising: 1) CB1 receptors in some species have even longer N-termini; 2) sequence conservation is extremely high within the transmembrane domains and parts (but not all) of the N-terminal domain, and 3) secondary structure predictions (using IUPred3) suggest the un-spliced N-terminus contain regions of intrinsic disorder.

Further analysis of only mammalian CB1 receptors (87 unique sequences from 62 CB1 homologs, and 9 CB1a and 16 CB1b splice variants) showed that CB1-NT has three apparent structural components conserved among mammalian CB1. The first ~ 22 residues are highly conserved, the following ~ 33 residues (residues 23-55) are non-conserved, and conservation increases again in the region from residue 55 to 116. An analysis of intrinsic order (not shown) suggests the conserved regions are likely ordered, and the non-conserved region more disordered, and thus prone to proteolysis. This is noteworthy as the human splice variant CB1b is missing residues 22-54, roughly the same region of low conservation/higher disorder shown in Figure 1.3.

The CB1 N-terminus affects receptor expression and cellular targeting. For example, CB1 N-terminal truncation mutants express better in cell culture³⁶⁻³⁸, as do CB1 splice variants (CB1a and CB1b) (19). As noted above, the first 22 residues of the N-terminus was proposed to contain a mitochondrial targeting sequence²⁹. Analysis of potential proteolytic sites in the CB1 N-terminus done in PROSPR and ExPASy's PeptideCutter show several potential cleavage sites (Figure 1.4). Of note, we often see proteolytic cleavage of the CB1 N-terminus in our expression systems. Similarly, the CB1 N-terminus contains putative N-linked glycosylation sites^{36,39,40}, as well as numerous potential O-linked glycosylation sites.

Unfortunately, there is currently no structure of the CB1 N-terminus to provide clues for its function – it is not resolved in any of the current CB1 structures, with only the first ~10 residues before the first helix (TM1) visible, either because deletion mutants were used, or because the region was not visible in the data. This is unfortunate, as the N-terminus may undergo some relatively large re-

arrangements during activation, including in the so-called membrane-proximal region (MPR) that has been implicated in allosteric regulation of CB1³⁵.

The role the CB1 N-terminus plays in receptor signaling has never been systematically studied, likely because much of it can be deleted without affecting binding of high affinity, synthetic ligands. However, CB1 crystal structures show a major difference between agonist and inverse agonist bound receptor – the location of the CB1-NT MPR⁴¹. For inverse agonists, the MPR forms a structured “cap” over the ligand binding pocket and makes several contacts with the ligand. In contrast, for agonist bound structures, the MPR makes few contacts with agonist ligands, and instead forms an extended structure that moves away from the binding pocket⁴¹. Previously, members of the Farrens lab found reducing the disulfide in the MPR (C98-C107) causes antagonist binding to *increase* and agonist binding to *decrease* (Figure 1.5), with more agonist necessary to activate G protein (not shown)³⁵. One way this unusual phenomenon could occur is if the CB1-NT and MPR bind and stabilize the inactive apo-state conformation. The resulting shift in equilibrium populations would explain the results above.

Lack of information about CB1 in general, and the N-terminus in particular, led us to assess how novel anti-CB1 antibodies could be used to study its structure and function, noted below.

1.5 Anti-CB1 antibodies

Prior to 2020, the majority of CB1 studies relied on polyclonal antibodies raised against peptides of the CB1 N-terminal region. Initial identification of a pre-synaptic population of CB1 was conducted with a polyclonal anti-CB1 N-terminal antibody²¹. In western blot studies, the apparent molecular weight of CB1 varies between 50 and 70 kDa^{36,42,43} depending on the antibody used to visualize the receptor. This discrepancy could be due to a number of factors including post-translational modification of the N-terminus, such as glycosylation or proteolysis, or due to splice variants.

New anti-CB1 polyclonal antibodies continue to emerge, including two well-validated, commercially available anti CB1 polyclonal antibodies that recognize residues 1-14 (Nt Cay) and 84-99 (Nt Alo) of the CB1 N-terminus³⁶. While these antibodies present an improvement from previous tools, there are limitations when using polyclonal antibodies. Generally, monoclonal antibodies are more consistent and reliable, particularly for structural studies including analysis of the post-translational landscape of a protein⁴⁴.

Novel anti-CB1 monoclonal antibodies were previously generated by Dr. Jon Fay in the Farrens lab and Dr. Dan Crawley (formerly OHSU VGTI) against a mutant CB1 lacking the first 88 residues of the N-terminus³⁷. An overview of the top candidates and their initial characterization is presented in Chapter 2. As described below, these novel monoclonal antibodies present new tools for examining the structure, function, and dynamics of CB1.

1.6 Overview of thesis

This thesis aims to address the need for novel tools and techniques to examine the structure, post-translational modification, and subcellular localization of GPCRs, in particular CB1. Chapter 2 details the characterization of several novel anti-CB1 monoclonal antibodies. Interestingly, one of these antibodies, called 1E10, seemed to only recognize the $\Delta 88$ CB1 truncation mutant, but not the full-length receptor or a full N-terminal deletion mutant. In this chapter, three top candidate antibodies were thoroughly characterized and validated for Immunoblot, immunoprecipitation, and immunofluorescence. For the 1E10 antibody, 10- and 4- residue tags were developed for final validation of the antibody epitope and both tags were validated for immunoblot and immunofluorescence, with one goal being application to study possible roles of the CB1 N-terminus, discussed below.

Chapter 3 discusses exploration of the role of the CB1 N-terminus and validation of tools for this purpose. Given the emerging interest in a potential intracellular or mitochondrial population of CB1 and

the length and potential for post-translational modification of the CB1 N-terminus, it is possible that the N-terminus is playing an important role in regulation of CB1 dynamics. Specifically, the main hypothesis of this chapter is that the CB1 N-terminus plays a role in receptor regulation or subcellular localization, potentially via post-translational modification such as glycosylation. While a high degree of receptor expression heterogeneity obscured results, several techniques were validated for examining surface expression and differential subcellular localization of CB1 using confocal microscopy.

Chapter 4 focuses on the development and improvement of protein immunoaffinity purification strategies. With my characterization of a novel antibody described in Chapter 2 came the opportunity to leverage this tool in existing protocols. Thus, 1E10 was used for immunoaffinity purification of several CB1 and tagged rhodopsin variants. Multiplexed peptides were tested with the goal to improve elution from immunoaffinity columns.

Final thoughts and conclusions are presented in Chapter 5. There are three appendices, one with the primers used to generate constructs used in this thesis and two with data obtained from Dr. Emily Platt relevant to the work of this thesis.

Figures:

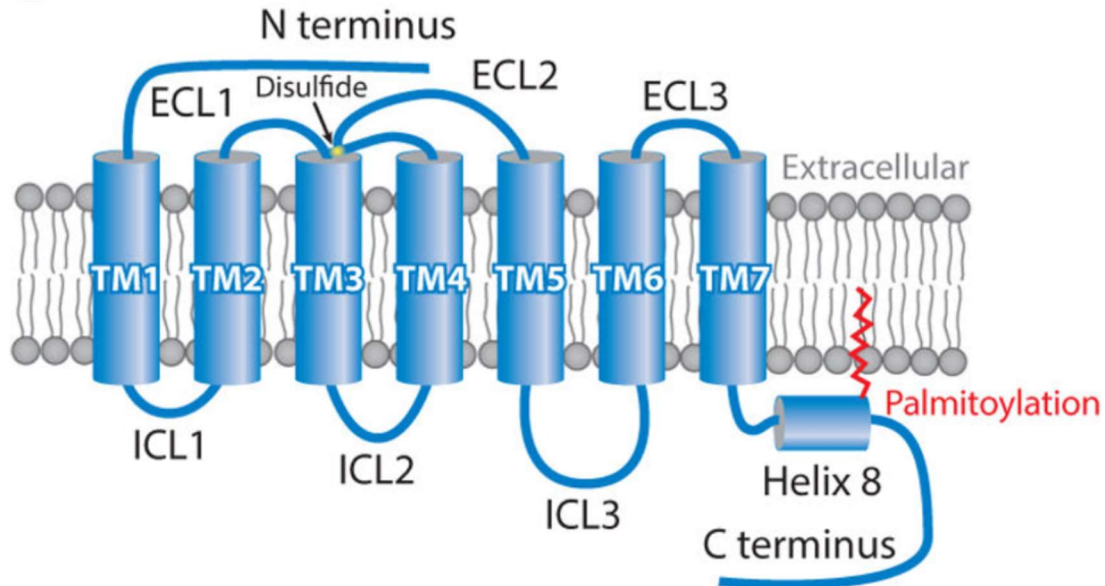


Figure 1.1: Schematic of GPCR structure. GPCRs contain seven transmembrane helices (TM1 – TM7).

Extracellular loops (ECL 1-3) and the N-terminus are located on the extracellular side of the lipid bilayer.

Intracellular loops (ICL1-3), helix 8, and the C-terminus are located on the intracellular side of the bilayer, the side where G proteins and other signaling proteins interact. Figure from ¹.

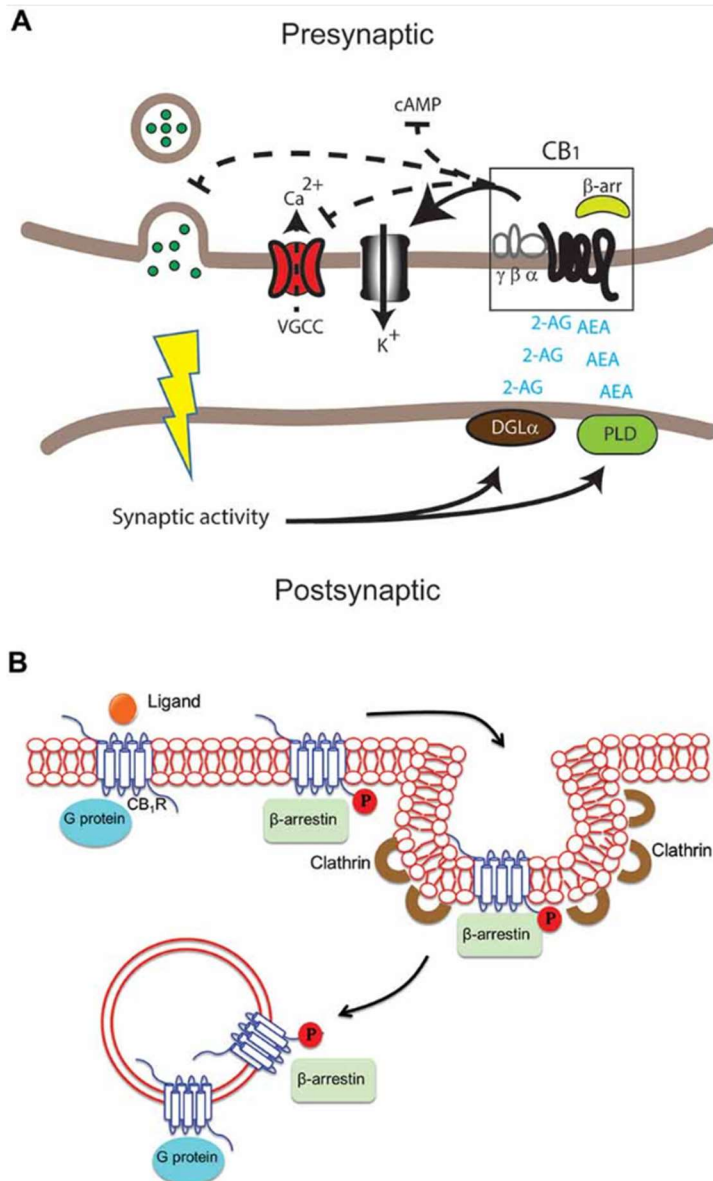


Figure 1.2: Schematic of CB1 signaling and internalization. **(A)** schematic of CB1 signaling.

Neurotransmitter release from the pre-synapse activates postsynaptic receptors which results in the production of endocannabinoids 2-AG and anandamide (AEA), which in turn activate CB1 resulting in inhibition of cAMP production, inhibition of Ca²⁺ influx, increased K⁺ efflux, and inhibition of neurotransmitter release from the pre-synapse. **(B)** β -arrestin binds activated CB1, leading to clathrin-mediated endocytosis of activated receptors. From: ²⁸.

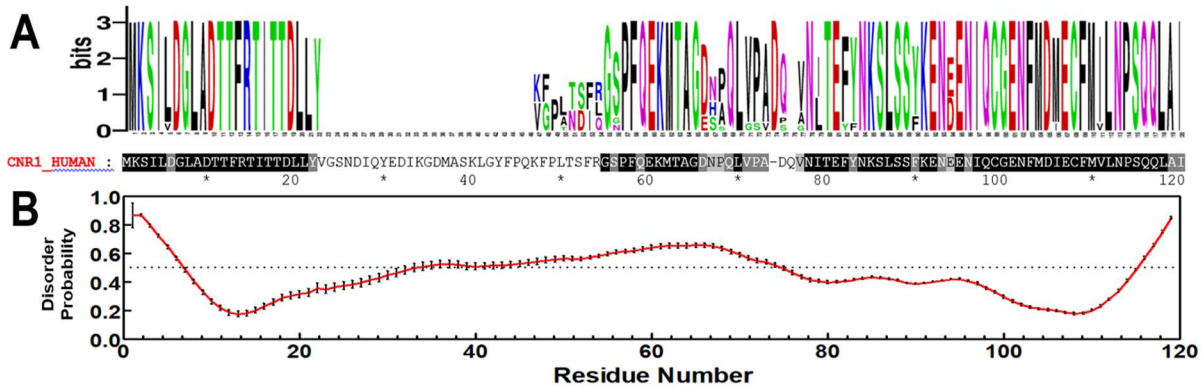


Figure 1.3: Sequence logos describing the different splice variants of mammalian CB1 N-termini detected in a multiple sequence analysis (MSA). At each position, the stack height denotes the level of sequence conservation, and the symbol height the frequency of each residue. **(A)** 87 unique orthologs of CB1 N-terminal sequences were extracted from the Uniprot database and used in the MSA. Most sequences have the ~120 residue highly conserved N-terminal domain, but 25 orthologs had shorter N-termini. **(B)** A plot of the disorder probability as a function of residue number predicts the non-conserved region may contain a higher degree of disorder. Source: Dr. Ujwal Shinde, PhD, OHSU Chemical Physiology and Biochemistry.

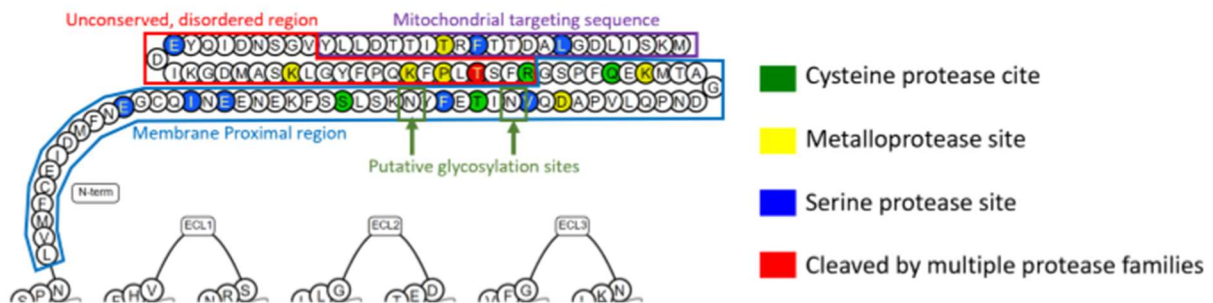


Figure 1.4: The CB1 N-terminus is predicted to undergo proteolytic cleavage and glycosylation. Figure generated using GPCRdb.org⁵. Putative proteolytic sites were identified with PROSPR, N-glycosylation sites using NetNGlyc-1.0. The non-conserved, putative disordered region is from Figure 1.3.

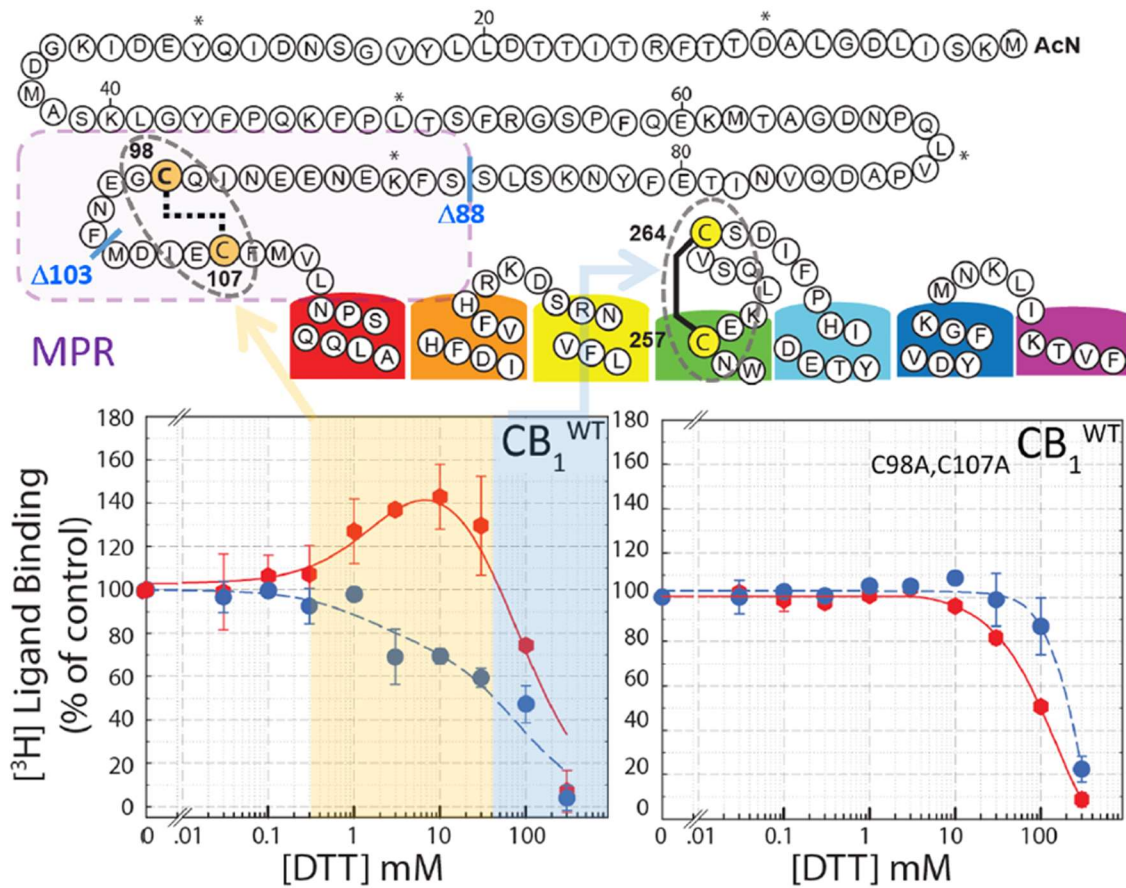


Figure 1.5: Cysteine residues in the membrane proximal region (MPR) of the CB1 N-terminus can modulate receptor-ligand interactions. The disulfides and MPR are indicated, as well as several truncation sites ($\Delta 103$, $\Delta 88$) previously tested for ligand binding. The allosteric effect the MPR has on the binding of inverse agonist (red) and agonist (blue) can be seen with reducing disulfides at C98-C107 and C257-C264. Figure was adapted from: ³⁵.

Chapter 2

2.1 Introduction

Previously, novel anti-CB1 antibodies were generated against a CB1 mutant for which both the N- and C-termini were deleted ($\Delta 88/\Delta 418$)^{37,45}. This mutant, called Goldilocks, or CB1-GL is shown in Figure 2.1A. CB1-GL, was used extensively for structural and biochemical work in the Farrens lab due to its better resistance to proteolysis and higher expression in mammalian tissue culture (Farrens et al., 2002). As most commercially available anti-CB1 antibodies are polyclonal antibodies that target the N-terminus of CB1, and CB1-GL lacks most of the N-terminus, the antibodies generated against this mutant CB1 were inherently novel.

Initial characterization of these antibodies was performed by Dr. Fay via slot blot on the five most promising novel anti-CB1 monoclonal antibodies (Figure 2.1). The top three candidates were then selected for further characterization and validation: 1E10, 3A3, and 5G3³⁷. All three antibodies were able to visualize as low as 5 ng of the receptor they were generated against (CB1-GL). Antibodies 3A3 and 5G3 did not bind a mutant lacking the intracellular loop 3 (IL3) region of CB1, but they bound all N-terminal mutants. These antibodies were therefore identified as binding an epitope in the IL3 region of the receptor. Interestingly, the 1E10 antibody bound both the mutant lacking IL3 region as well as N-terminal truncation mutants ($\Delta 88$ only) but did not detect full-length receptor or a mutant receptor lacking the entire N-terminus. These results suggested that the 1E10 antibody binds an N-terminal epitope of the truncated receptor these antibodies were raised against (CB1-GL).

In this chapter, I describe my more detailed characterization of these three antibodies, as well as their validation for immunoblot, immunoprecipitation, and immunofluorescence. Furthermore, for one of these antibodies, 1E10, I developed small (10- and 4-) residue tags and validated their use for immunoblot and immunofluorescence studies.

2.2 Methods

Buffers:

RIPA buffer: 50 mM Tris pH 7.8, 1 % Nonidet P-40, 0.5 % deoxycholate, 150 mM NaCl, 5 mM EDTA.

Protease inhibitors: 1X Halt (Thermo Fischer Scientific), 5 µg/ml leupeptin, 0.5 mM PMSF.

4X sample buffer: 8.0% SDS, 40% glycerol, 0.25 M Tris pH 6.8, 0.02% - 0.04% BPB.

Mutants:

Three CB1 mutants are used throughout this work, all designed and described previously. Briefly, shCB1-C2 is a full-length synthetic human CB1 with only two cysteine residues (C257 and C264) which form a disulfide⁴⁶. CB1-GL (also referred to as GL) is an N- and C-terminal truncation (Δ87 and Δ417) mutant of shCB1-C2^{37,38}. CB1-ΔIL3 (also referred to as ΔIL3) is a modified shCB1-C2 with an N-terminal truncation (Δ87 like GL) with IL3 deleted³⁷. All mutants have the last 8 amino acids replaced with the 1D4 epitope (TETSQVAPA) for detection and purification.

Mutant/construct generation:

PCR conditions are located in tables 2.2-2.4. Overlap extension PCR was performed according to Heckmen and Pease⁴⁷ and is summarized in tables 3 and 4. Primers for PCR can be found in Appendix 1. PCR was validated by running 5 µL PCR products on 1% Agarose DNA gel at 60 V for 1 hour.

PCR products were digested with relevant restriction enzymes in a double digest. Appropriate units of restriction enzyme were added to remaining PCR products along with relevant NEB reaction buffer to a total volume of 60 µL. Samples were incubated at 37 °C for 1 hour, then cleaned on a QIAquick spin column. Concentrations of cleaned PCR products were estimated using Nanodrop.

Linearized vector was prepared by digesting vector construct with two restriction enzymes. 5 µg vector construct was digested with 2 units (1 µL) of each restriction enzyme in 1X NEB 3.1 buffer or CutSmart (NEB) buffer (40 µL total volume). Sample was incubated for 90 minutes, then 1 µL Cow Intestinal Phosphatase (CIP) was added and sample was incubated at 37 °C for an additional 30 minutes.

The sample was run on a 1% Agarose DNA gel at 60 V for 1 hour. Vector band was cut out and purified using QIAquick spin columns (QIAquick gel purification kit protocol). Concentrations of linearized vector were estimated using Nanodrop.

Linearized vector and digested insert from PCR (~1:3 ratio) was added to 1X T4 ligase buffer to a total volume of 19 μ L. 1 μ L T4 ligase was added, and samples were incubated for 2 hours at 25 °C. 2 μ L of ligation product was added to 50 μ L of DH5-alpha cells. Samples were incubated on ice for 30 minutes, then 42 °C for 45 seconds, then on ice for two minutes prior to plating on prepared LB agar plates + 100 μ g/mL Ampicillin. Plates were incubated overnight at 37 °C.

Mini prep and sequencing:

1-2 colonies from each plate were gently removed with a p200 pipette tip and placed in 5 mL LB + 100 μ g/mL Ampicillin. Samples were incubated at 37 °C and 200 rpm for 18-20 hours. Then ~ 1 mL of each sample was transferred to a 1.5 mL Eppendorf and mini prep was performed using the Qiagen Mini Prep protocol. The concentration of each sample was estimated using Nanodrop. At least 500 ng DNA from each sufficiently concentrated sample was then prepared and submitted for sequencing.

Antibody generation:

As noted above, mouse monoclonal anti-CB1 antibodies were generated previously by Dr. Jon Fay (former graduate student in the Farrens lab) and Dr. Dan Crawley (formerly at VGTI)³⁷. These antibodies were generated against a CB1 mutant with N- and C- terminal truncations (CB1 Δ 88/ Δ 418, also called CB1-GL)^{46,48}

Transfection/Harvesting:

Cos-1 cells were seeded onto a 150 mm tissue culture dish and grown until confluent. 30 μ g of DNA was added to 2.5 mL Optimem and incubated for 5 minutes at room temperature. 100 μ g PEI was added to 2.5 μ L Optimem and incubated for 5 minutes at room temperature. Then DNA and PEI solutions were mixed and incubated for 20 minutes at room temperature. Media was aspirated from

plates and 15 mL fresh media was added. 5 mL DNA/PEI/Optimem mix was added per plate. Plates were incubated for 50-65 hours prior to harvesting. To harvest, media was aspirated and cells were washed twice with 10 mL PBSSC. Then cells were gently scraped into 2 mL PBSSC and placed in 15 mL conical vial. Cells were then pelleted by centrifugation (10 min at 4 clicks on a clinical centrifuge) and stored at -80 °C.

After cells were harvested and pelleted, they were solubilized in RIPA buffer + protease inhibitors, then pelleted at 14,000 rpm in the eppendorf centrifuge at 4 °C. Supernatants were removed, aliquoted and stored at -80 °C.

Immunoprecipitation:

50 µg total protein were added to RIPA + protease inhibitors up to 100 µL for each construct. Antibodies were added at specified final concentrations, and samples were incubated at 4 °C for 10 minutes. Then 25 µL 50% slurry of Protein A sepharose beads in RIPA + protease inhibitors was added to each sample. Samples were incubated for 90 minutes at 4 °C, then washed 3 times with 5 column volumes RIPA + protease inhibitors. Samples were eluted in 25 µL 1X sample buffer + 0.1 M DTT at 37 °C or 65 °C for 30 minutes (CB1 mutants) or 25 °C for 30 minutes (rhodopsin mutants). Samples were loaded onto an 8% acrylamide gel. For control lanes, cell extracts were prepared with ~10 µg total protein in 1X sample buffer + 0.1 M DTT and incubated at 65 °C for 30 minutes or added directly to the gel. Gels were run at 50 V until tracking dye (BPB) had run off the bottom of the gel. Samples were transferred to PVDF membrane at 190 mA for ~1 hour. The membrane was incubated with primary antibody at 1/1000 dilution (~5 µg/mL for 1D4, 1E10, 3A3, and 5G3) and goat-anti-mouse AF680 secondary antibody at 1/5000 dilution. Images were captured on Sapphire Imager, processed with ImageJ, and labeled using Inkscape. Specific imaging conditions were dependent on the fluorophore used. All images were captured with an intensity setting that did not result in saturation.

Peptide competition immunoprecipitations:

Antibodies were incubated with varying concentrations of peptide (as indicated) for 30 minutes at 4 °C in RIPA + protease inhibitors. Peptides can be found in Table 2.5. Then 50 µg total protein was added to each sample and immunoprecipitation protocol proceeded as described above.

Immunofluorescence:

Cos-1 or HEK 293 cells were transiently transfected as previously described onto poly-L-lysine treated coverslips in a 12-well plate. Cells were fixed with 4% formaldehyde in 1X PBSSC, then blocked and permeabilized with 4% horse serum, 0.1% Triton-X100, 1X PBSSC, then washed once with 1X PBSSC. Primary antibody (1E10 or 1D4) was incubated in a 0.1% Tween-20, 1X PBSSC buffer for 1 hour at room temperature in a humidified container to prevent evaporation. After three 5-minute washes with 0.1% Tween-20, 1X PBSSC, the samples were incubated with secondary antibody (Goat-anti-mouse AF488) in the same buffer for 1 hour at room temperature. Coverslips were washed three times with 0.1% Tween-20, 1X PBSSC then three times with 1X PBSSC. Coverslips were mounted to glass slides with VectaShield mounting solution with DAPI, then sealed with clear nail polish. Slides were imaged on a Zeiss Apotome 3 using the 63X oil objective. Images were processed in ImageJ.

2.3 Results

Characterization and validation of intracellular binding antibodies, 3A3 and 5G3.

Characterization of the epitopes of the three top antibody hits was accomplished through a series of peptide competitions, deletions, and mutations. First, peptide corresponding to the middle of IL3 (SIIHTSED) was assessed for its ability to compete with binding of the ICL3 antibodies (3A3 and 5G3). This competition was not successful at any of the concentrations tested (Figure 2.2A). A series of deletions in the IL3 was used to identify a large region of the loop as a putative epitope (Figure 2B). These deletions consisted of three overlapping deletions of 10 residues each. While the first deletion reduced affinity of both antibodies, the second deletion fully prevented antibody binding to the mutant

receptors. This indicates that the epitope of both antibodies is in the N-terminal half of IL3. Final determination of the epitopes of the 3A3 and 5G3 antibodies was conducted via immunoblot of grouped alanine scans (Figure 2.2C and 2.2D), revealing the epitope for both antibodies consists of no more than residues HITS EDGKVQ, and possibly less. These epitopes were confirmed using immunoprecipitation (Figure 2.2C and 2.2D). Together, these data reveal the epitopes of each of the two IL3 binding antibodies and validate their use in immunoblot and immunoprecipitation.

Characterization and validation of an N-terminal binding antibody, 1E10. The identity of the 1E10 antibody epitope was determined with immunoprecipitation studies carried out in increasing concentrations of peptide containing the putative 1E10 epitope (SFKENEENIQ; Figure 2.3A). At all concentrations of peptide tested, binding of antibody to CB1-GL was blocked, preventing immunoprecipitation (Figure 2.3A and 2.3B). N-terminal peptide did not block binding of 3A3 at any concentration tested, confirming this is a specific interaction between the peptide and antibody. Together, this indicates that the epitope is contained in the region represented by the N-terminal peptide (SFKENEENIQ). Immunoprecipitation of a mutant with a single glycine addition to GL (CB1-GL G88) was competed by similar concentrations of N-terminal peptide (Figure 2.3B).

Detailed alanine scan of 1E10 epitope for final characterization of 1E10. To further localize and identify key residues in the epitope required for 1E10 binding, an alanine scan of the region was performed, in which two residues at a time were mutated to alanine. Solubilized membranes of alanine mutants were probed with 1D4 as an expression control or 1E10. This scan indicated that the first four residues (SFKE) had the greatest impact on 1E10 binding (Fig. 1.3C). To further identify the contribution of these four residues, each of these residues individually mutated to alanine. These four single alanine mutants were expressed, their membranes solubilized, then probed with 1D4 or 1E10 as in the previous scan (Figure 2.3D). These results indicate that S88 and F89 play the largest role in the binding interaction with K90 and E91 also contributing.

I next tested if N-terminal acetylation is required for 1E10 binding to the epitope. Peptides were ordered with the putative epitope region (SFKE) with or without N-terminal acetylation. Given the results of the previous alanine scan, an N-terminally acetylated peptide corresponding to the E91A (Figure 2.3D) mutant (SFKA) was also included. Each peptide was tested for its ability to compete in the peptide competition IP as described above. While the N-terminally acetylated SFKE peptide was able to compete with CB1-GL for binding to 1E10, neither the non-acetylated SFKE nor the acetylated SFKA peptide were able to compete (Figure 2.4A). These data strongly suggest that the 1E10 epitope includes N-terminal acetylation. This could explain why 1E10 does not recognize full-length receptor, as this processing would not occur at the epitope region in full-length receptor.

In order to assess if cleavage of the start methionine was necessary prior to acetylation, a similar experiment was conducted with an N-terminally acetylated MSFKE peptide and a non-acetylated MSFKE peptide. Neither methionine-containing peptide was able to compete 1E10 binding to CB1-GL (Figure 2.4B). These results strongly suggest that the complete 1E10 epitope requires the initiator methionine be cleaved followed by N-terminal acetylation of the following residue (serine). Together, these data firmly identify the epitope of 1E10 while also validating this antibody for use in immunoblot and immunoprecipitation.

Validation of antibodies for use in immunofluorescence studies. The three antibodies (5G3, 3A3 and 1E10) were then validated for use in immunofluorescence studies (Figure 2.5). The results show the antibodies were able to visualize the CB1-GL receptor at 1:500 and/or 1:500 dilutions (from 1 mg/mL). Both 3A3 and 1E10 were able to visualize transiently transfected protein at both dilutions (Figures 2.5A and 2.5B). 5G3 was able to visualize receptor well at 1/500 dilution (Figure 2.5C). All three antibodies were successful at visualizing transiently transfected protein in immunofluorescence.

Generation and validation of 10- and 4- residue N-terminal tags for use with 1E10 antibody. Final confirmation of the 1E10 epitope was obtained by introducing it as a 10 residue (SFKENEENIQ) or 4

residue (SFKE) addition onto the N-terminus of another class A GPCR, rhodopsin (Figure 2.6A). Solubilized membranes expressing both constructs could be visualized with 1E10 (Figure 2.6B). Importantly, the data show that the banding pattern of the 4-residue addition was analogous to that observed for wild-type rhodopsin. This suggests that glycosylation of the 4-residue tagged rhodopsin is similar to wild-type receptor, indicating this small epitope did not egregiously impact receptor folding. This is an important point, as rhodopsin is known to be glycosylated at N2⁴⁹. Similarly, the 4-residue addition had less impact on the ability of receptor to photo-activate (Figure 2.6C). Finally, the specificity of the 1E10 for the epitope was demonstrated by immunofluorescence studies of the SFKE-Rho and shRho transiently transfected in HEK 293 and visualized using 1D4 or 1E10 immunofluorescence (Figure 2.6D). 1E10 was able to visualize the SFKE-tagged rhodopsin, but not the wild-type receptor, whereas the 1D4 staining detected both receptors expressed. Together, these results indicate that both the 10- and 4-residue additions can act as a visualization tag for immunoblots.

2.4 Discussion

Anti-CB1 monoclonal antibodies were generated, and the top three candidates were extensively characterized and validated for immunoblot, immunoprecipitation, and immunofluorescence. Two of these antibodies (3A3 and 5G3) bind an intracellular epitope, whereas 1E10 binds a specific and short epitope in the N-terminus of the receptor. All antibodies were validated for use in immunoblot, immunoprecipitation, and immunofluorescence.

For final characterization of the 1E10 epitope, my peptide competition immunoprecipitation experiments were repeated with an acetylated and non-acetylated SFKE peptide as well as two peptides with the sequence MSFKE, the latter to assess if cleavage of the initiator methionine was needed for optimal 1E10 epitope. While the N-terminally acetylated SFKE peptide was able to compete 1E10 binding to CB1-GL similarly to the full 10-mer peptide, neither the non-acetylated SFKE nor the acetylated SFKA

peptide were able to compete binding, indicating that the acetyl group is part of the antibody epitope. My data (Figure 2.4) strongly suggests this structure requires co-translational processing of the N-terminus, including cleavage of the start methionine and/or N-terminal acetylation. It is likely that the N-terminus of the truncated CB1 mutants or tagged mutants would undergo one or both of these modifications based on the sequence of its N-terminus^{50,51}. Neither MSFKE peptide was able to compete 1E10 binding to CB1-GL (Figure 2.4B), indicating that the start methionine is cleaved. Together, these data indicate that the start methionine of CB1-GL is cleaved then the N-terminus is acetylated when expressed and that this processing is necessary to create the 1E10 epitope. While the acetylated SFKE peptide was able to compete, it was not as effective as the full 10-mer peptide, indicating that the additional residues after SFKE may contribute to the antibody-epitope interaction to a lesser extent.

My results also help explain why the 1E10 antibody does not detect proteolytically cleaved CB1 fragments, some of which produce the 1E10 epitope. In studies of CB1 with a full-length N-terminus, Dr. Emily Platt found the CB1 N-terminus can be cleaved by cellular proteases, with a major site of cleavage occurring directly after residue 87, thus producing the 1E10 epitope – SFKENE (unpublished Edman sequencing data from Emily Platt, Appendix 2). However, this cleavage product is not detected in Western Blots using the 1E10 antibody. My discovery that the 1E10 epitope requires an N-terminal acetylation now explains this puzzling observation. The proteolytically cleaved fragment may start with the correct sequence for 1E10 (SFKENE), but the process of proteolysis would not introduce an N-terminal acetyl group, and thus not be detected by 1E10. My results would also explain why 1E10 has not been able to visualize full-length receptor from rat brain or transiently transfected mammalian cell lines (HEK or Cos-1). If co-translational modification, such as N-terminal acetylation, is required for the 1E10 epitope, as my data suggests, 1E10 may not be able to visualize any cleaved receptor without this modification.

Finally, it was confirmed that the 1E10 epitope could be successfully added to and used to probe another receptor, in this case, rhodopsin. Both 10- and 4-residue epitope tags were generated for use with 1E10 and validated for immunoblot and immunofluorescence. The 4-mer tag had less impact on receptor activation than the 10-mer tag. This could indicate that this tag could work for proteins that have previously been sensitive to tagging at the extreme N-terminus.

2.5 Future Directions

Next steps for these antibodies could include sequencing of the antibodies and recombinant expression. Given their success in multiple antibody-mediated visualization systems, they could also be validated for use in immunohistochemistry. Finally, these antibodies can be used to probe the function, expression, modification, and subcellular localization of CB1 – as explored in Chapter 3 – as well as for use in immunoaffinity purification, as described in Chapter 4.

2.6 Figures

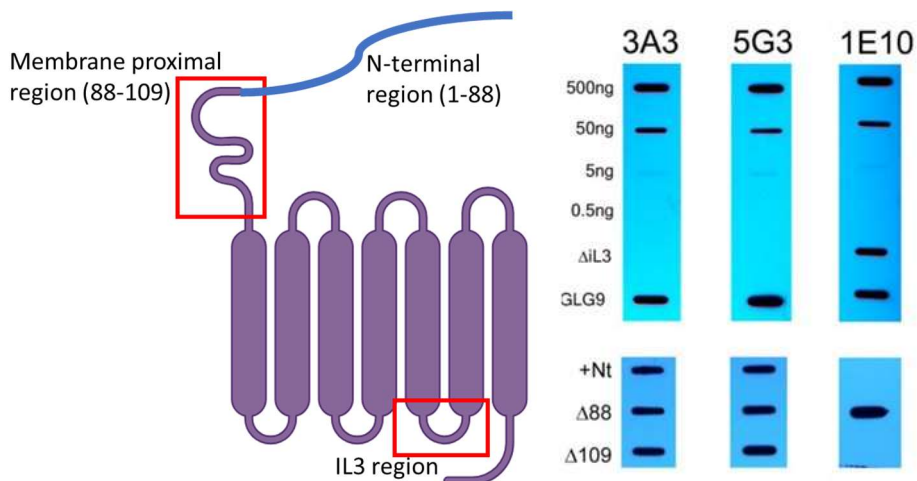


Figure 2.1: Schematic of CB1 with relevant regions highlighted (left). N-terminal segment, represented by the blue line, is residues 1-88. The membrane proximal region, marked with the red box, contains residues 88-109. The IL3 region is also marked with a red box Slot blot of various CB1 mutants imaged

with anti-CB1 antibodies as indicated (right),³⁷. This slot blot probes the ability of the three antibodies, 1E10, 3A3, and 5G3 to recognize decreasing concentrations of CB1-GL³⁸, (top 4 lanes, GLG9, and Δ88) a mutant shCB1-GL lacking the entire IL3 region, a full-length receptor (+NT), and a mutant lacking the full N-terminus including the membrane proximal region (Δ109).

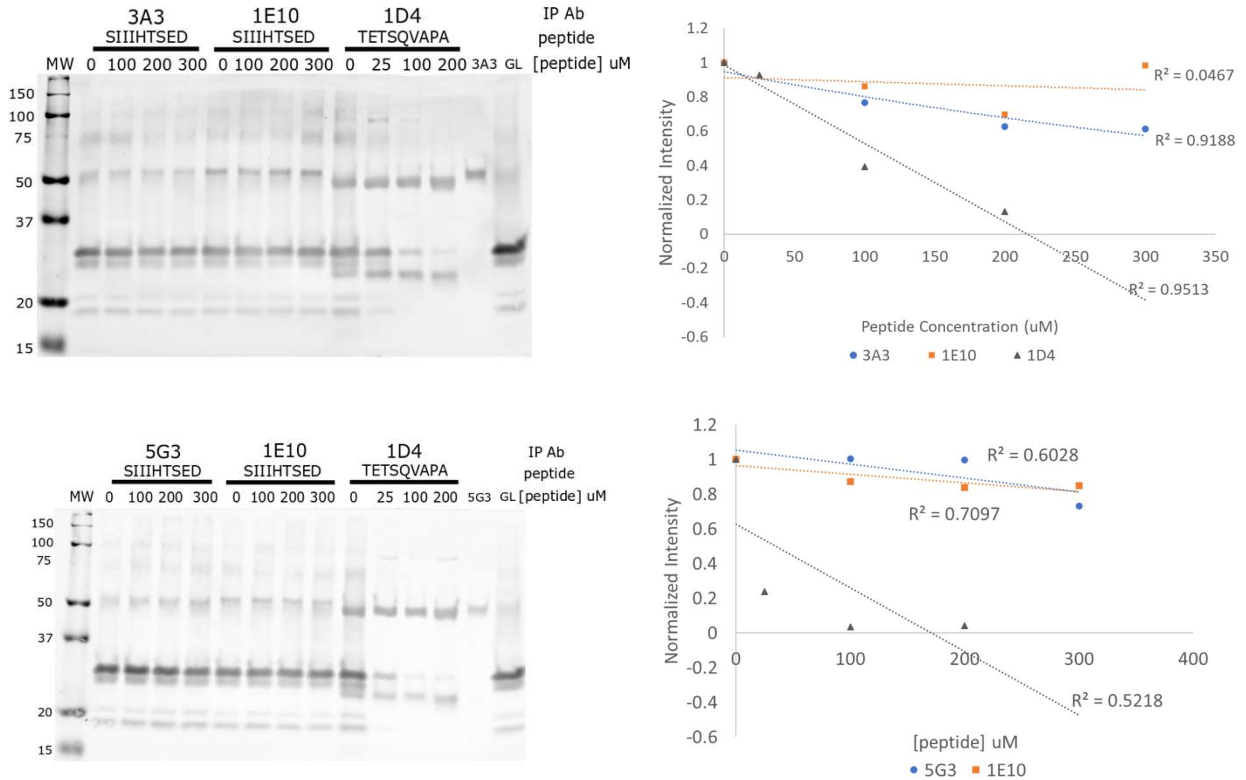


Figure 2.2A: Peptide competition IP of 3A3 (top) and 5G3 (bottom) with quantitation. 3A3, 5G3, 1E10, or 1D4 were incubated with various concentrations of noted peptide for 30 minutes prior to protein A immunoprecipitation of CB1-GL. As a negative control, 1E10 competed with IL3 peptide is included in each competition immunoprecipitation. 1D4 competed with its corresponding peptide is included in each as a positive control. 1D4 antibody heavy (~50 kDa) and light chain (~25 kDa) bands are slightly offset relative to 5G3 bands. Western blot lanes were quantified in ImageJ and data plotted in Microsoft Excel.

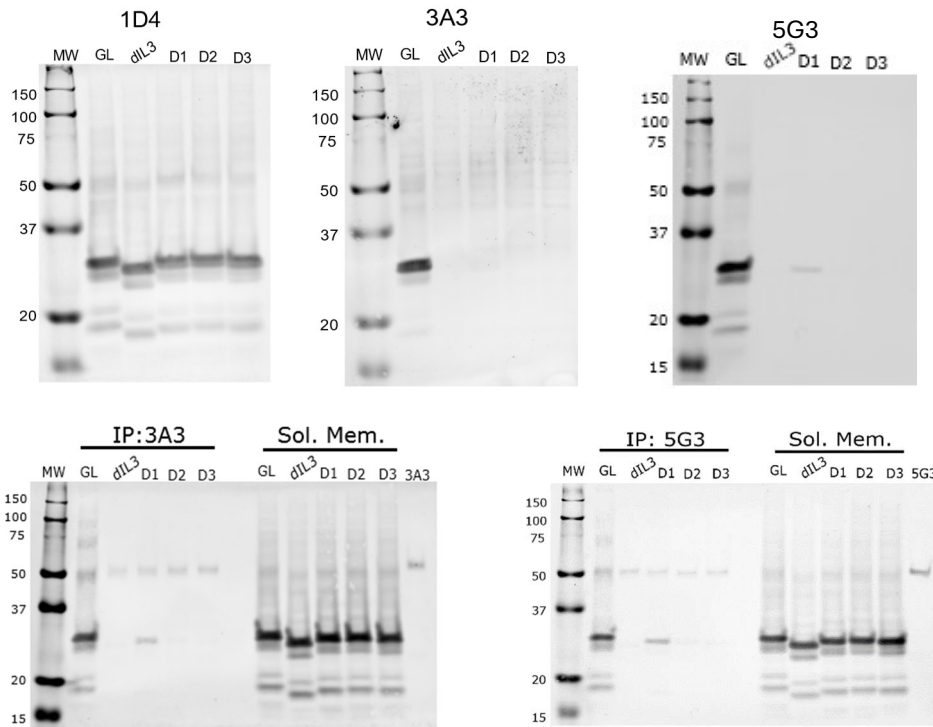
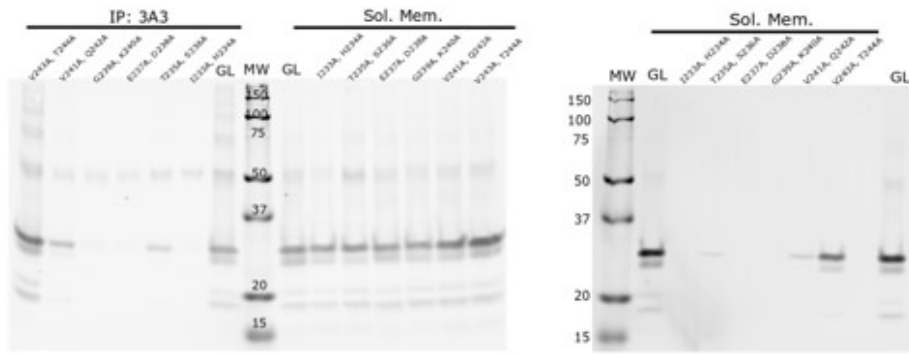


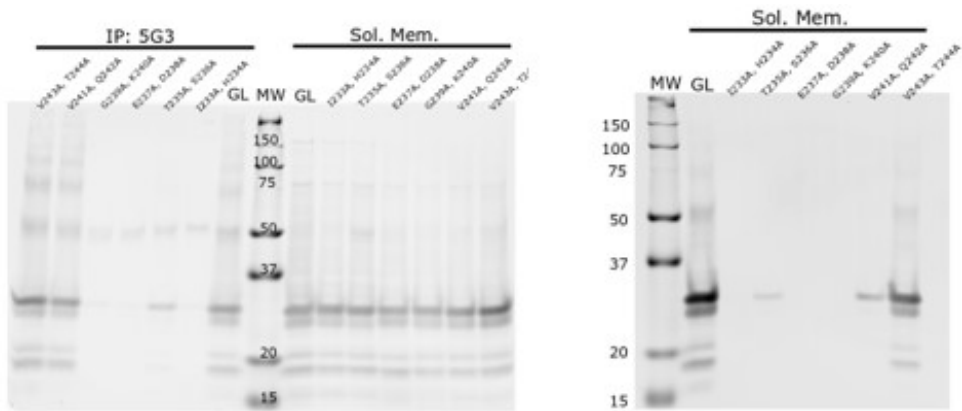
Figure 2.2B: IL3 deletion mutant western blots (top: 1D4 left, 3A3 center, 5G3 right). Δ IL3 (Δ IL3) lacks the entire CB1 intracellular loop 3 while deletion mutants D1, D2, and D3 contain overlapping 10-residue deletions. Immunoprecipitation with 3A3 (bottom left) and 5G3 (bottom right) by protein A were visualized with 1D4. RIPA solubilized membrane (Sol. Mem.) was included as an expression control in immunoprecipitation westerns.



Primary Ab: 1D4

3A3

Figure 2.2C: Double alanine scan of IL3. Solubilized membranes (Sol. Mem.) applied to gel, membranes probed with 1D4 (middle) or 3A3 (right). Protein A immunoprecipitation of double alanine mutants (left) with 3A3 was imaged with 1D4.



Primary Ab: 1D4

5G3

Figure 2.2D: Double alanine scan of IL3. Solubilized membranes (Sol. Mem.) applied to gel, membranes probed with 1D4 (middle) or 5G3 (right). Protein A immunoprecipitation of double alanine mutants (left) with 5G3 was visualized with 1D4.

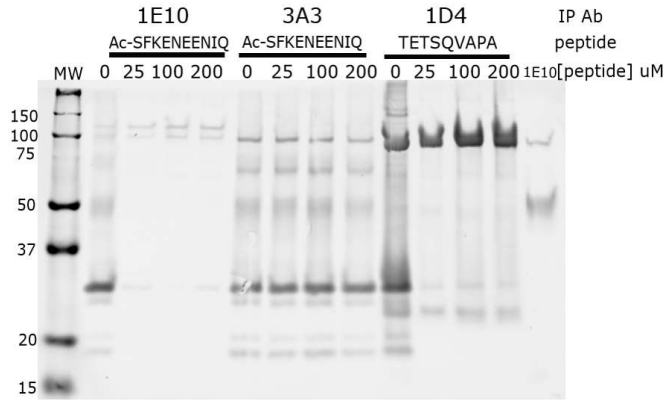


Figure 2.3A: Peptide competition of immunoprecipitation of CB1-GL with 1E10. 1E10, 3A3, or 1D4 were incubated with various concentrations of noted peptide for 30 minutes prior to protein A immunoprecipitation of CB1-GL. 3A3 competed with N-terminal peptide (SFKENEENIQ) is included as a negative control. 1D4 competed with its corresponding peptide is included in each as a positive control.

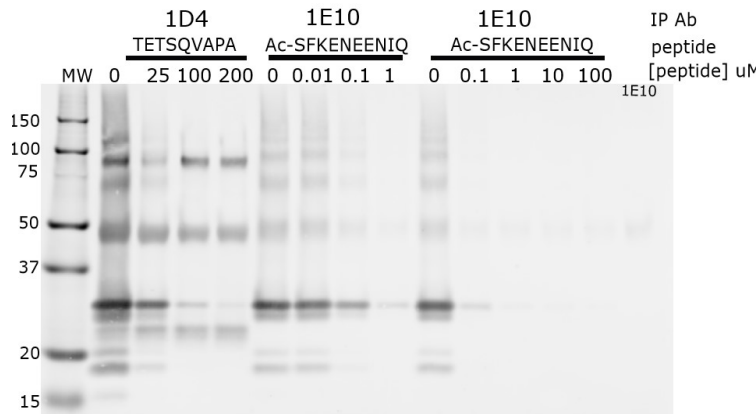


Figure 2.3B: Peptide competition of immunoprecipitation of CB1-GL (left and right groups) or CB1-GL G88 (center group) at various peptide concentrations. 1E10 or 1D4 were incubated with various concentrations of noted peptide for 30 minutes prior to protein A immunoprecipitation of CB1-GL (left and right) or CB1-GL G88 (center). 1D4 competed with its corresponding peptide is included in each as a positive control.

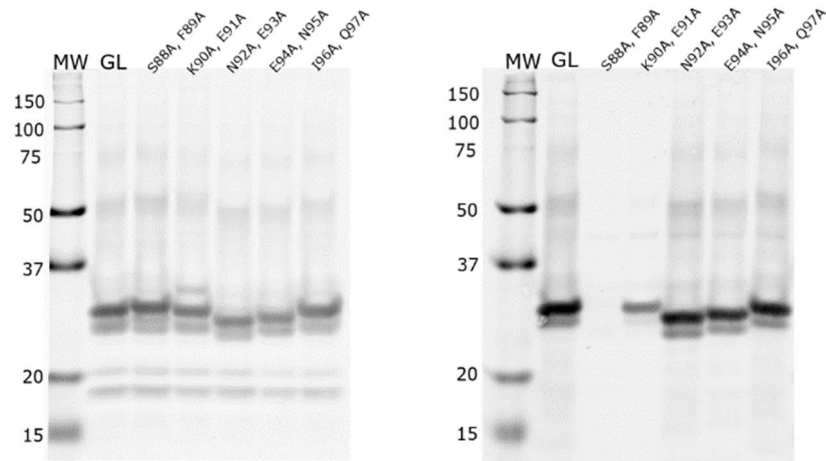


Figure 2.3C: Dual alanine scan of CB1-GL mutants map the requirements of the 1E10 epitope. Cell pellets were solubilized in RIPA, and solubilized membranes were run on gels and visualized with 1D4 (left) or 1E10 (right) western blots.

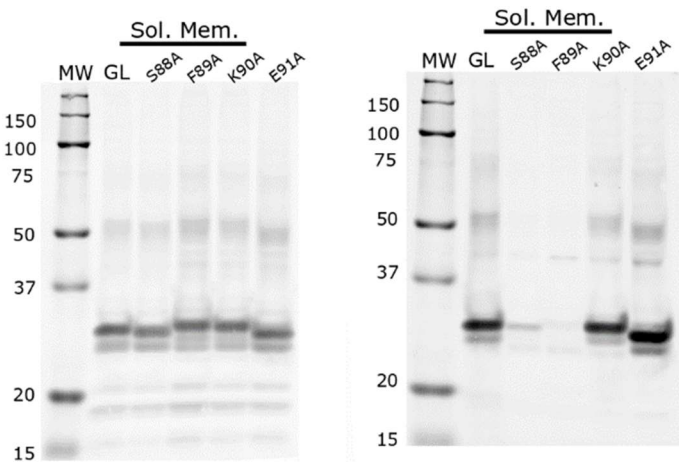


Figure 2.3D: Single alanine scan of CB1-GL mutants identify key residues in the 1E10 epitope. Alanine mutants of the putative 1E10 epitope in CB1-GL were generated and expressed in Cos-1 cells. The membranes were then solubilized and applied directly to gels for protein with Western blots, using 1E10 (right) or 1D4 (left) as an expression control.

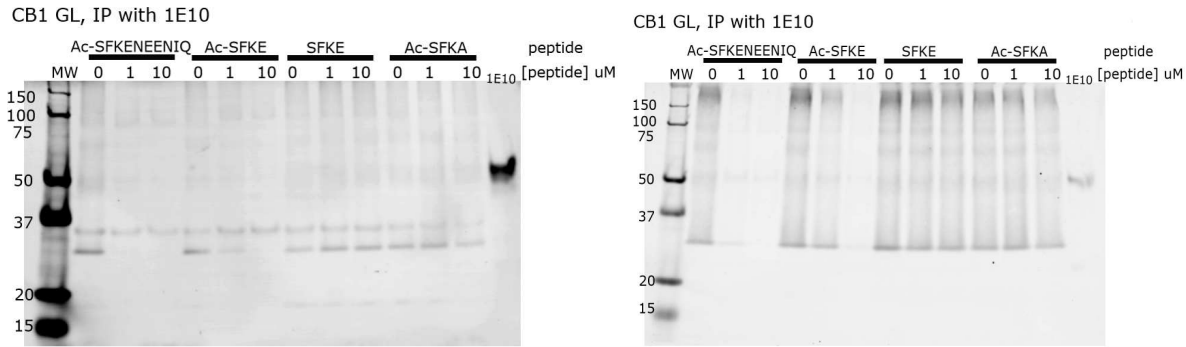


Figure 2.4A: Peptide competition studies indicate N-terminal acetylation is needed for the 1E10 epitope peptides to compete with 1E10 binding. Studies used CB1-GL with 1E10 and the various short peptides indicated. 1E10 was incubated with various concentrations of noted peptide for 30 minutes prior to protein A immunoprecipitation of CB1-GL. Ac-SFKENEENIQ is N-terminally acetylated. Ac-SFKE is N-terminally acetylated SFKE peptide, SFKE is non-modified SFKE, and Ac-SFKA is N-terminally acetylated SFKA peptide. Western blots were visualized with 1D4 (left) or 1E10 (right). Blots represent separate experiments.

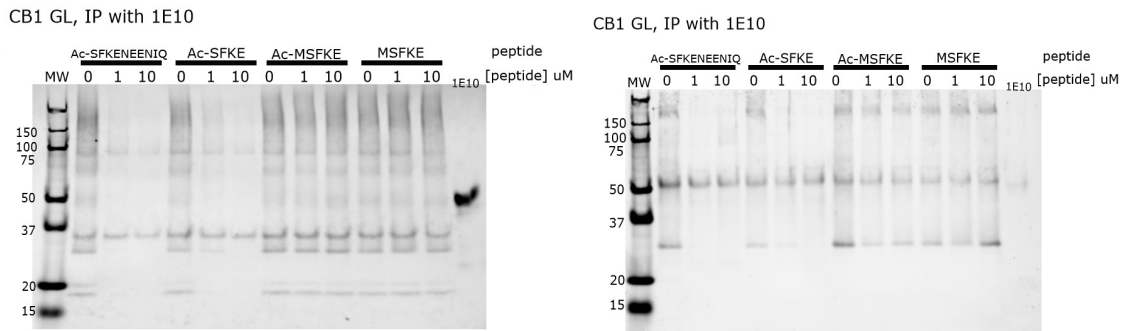


Figure 2.4B: Peptide competition immunoprecipitation with CB1-GL with 1E10 and short peptides with methionine. 1E10 was incubated with various concentrations of noted peptide for 30 minutes prior to protein A immunoprecipitation of CB1-GL. Ac-SFKENEENIQ is N-terminally acetylated. Ac-SFKE is N-terminally acetylated SFKE peptide, Ac-MSFKE is N-terminally acetylated MSFKE peptide, and MSFKE is non-modified MSFKE peptide. Western blots were visualized with 1D4 (left) or 1E10 (right). Blots represent separate experiments.

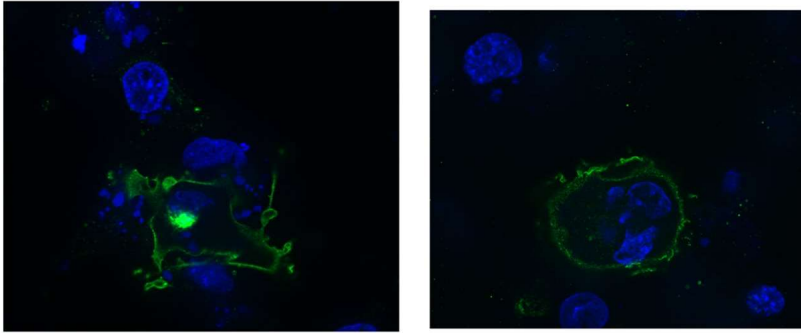


Figure 2.5A: Immunofluorescence of CB1-GL with 1E10. CB1-GL expressed in Cos-1 cells visualized with 1E10 at 1/500 (1 µg/mL, left) or 1/5000 (0.1 µg/mL, right).

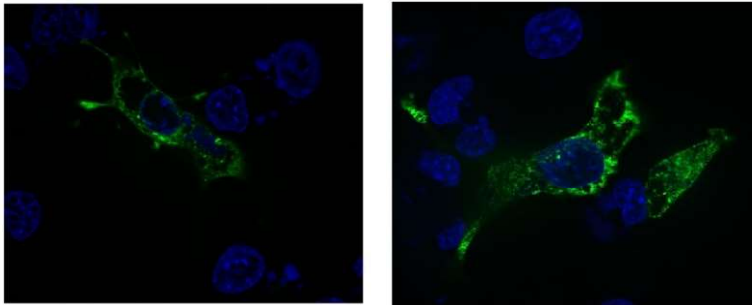


Figure 2.5B: Immunofluorescence of CB1-GL with 3A3. CB1-GL expressed in Cos-1 cells visualized with 3A3 at 1/500 (1 µg/mL, left) or 1/5000 (0.1 µg/mL, right).



Figure 2.5C: Immunofluorescence of CB1-GL with 5G3. CB1-GL expressed in Cos-1 cells visualized with 5G3 at 1/500 (1 µg/mL).

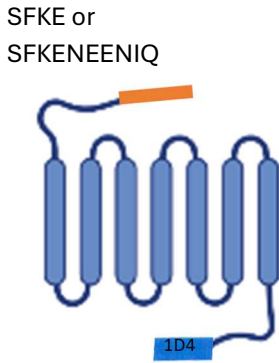


Figure 2.6A: Schematic of 10- and 4- residue additions corresponding to the 1E10 epitope to the N-terminus of rhodopsin. Yellow box at the N-terminus corresponds to the residues added (SFKE or SFKENEENIQ). Blue strand and ovals represent rhodopsin. Blue box at the C-terminus corresponds to the 1D4 epitope.

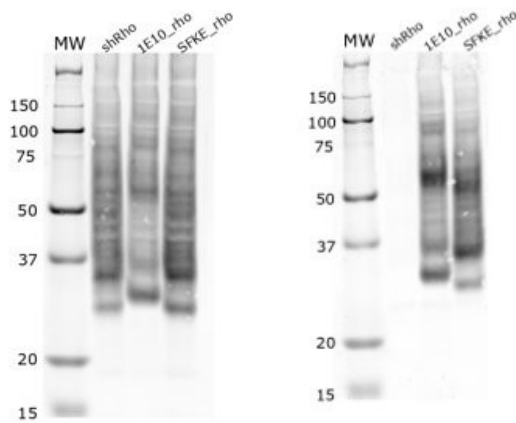


Figure 2.6B: 10- and 4- residue tags for visualization with 1E10. 1D4 (left) or 1E10 (right) was used to visualize shRho and tagged shRho mutants in western blot.

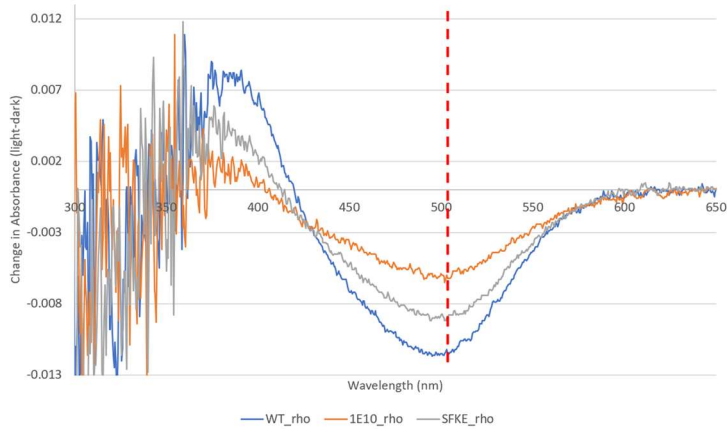


Figure 2.6C: Difference spectra of shRho and tagged-shRho mutants. Absorbance was measured for 80-90 μ L solubilized membranes (15 cm plate in 1 mL 1X PBSSC + 1% dodecylmaltoside) in the dark state (inactivated), then photobleached (activated) on a Shimadzu 1601 spectrophotometer. Absorbance spectra of dark (inactivated) rhodopsin was subtracted from the absorbance spectrum of light activated rhodopsin. Blue line represents the difference spectrum for shRho (WT rhodopsin), grey line represents the difference spectrum for SFKE-Rho, and the orange line represents the difference spectrum for 1E10-Rho. The magnitude of the change can be used to assess the amount of functional receptor produced that regenerated with the light-sensitive ligand 11-cis retinal.

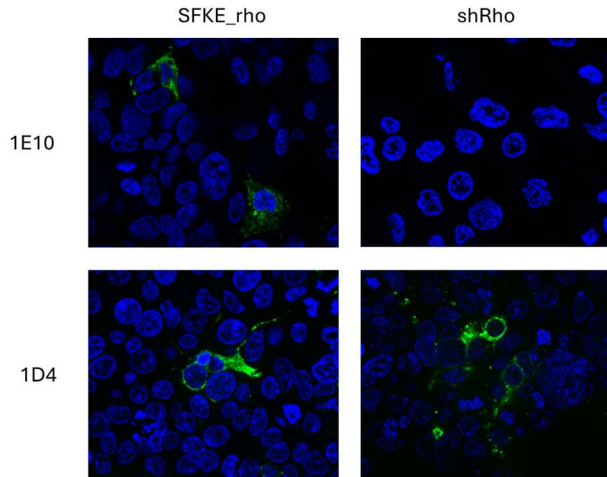


Figure 2.6D: Immunofluorescence of transient transfection of 4- residue addition mutant rhodopsin (left) or shRho (right) stained with 1E10 (top) or 1D4 (bottom). SFKE-Rho or shRho were transiently transfected into HEK 293 cells on coverslips without addition of large-T antigen plasmid (pRSV plasmid). Cells were stained with 1E10 or 1D4 and a goat-anti-mouse AF488 secondary antibody. Confocal images were collected on a Zeiss Apotome 3 confocal microscope at 63X magnification.

2.7 Tables:

Table 2.1: CB1 Monoclonal Antibody concentrations and remaining aliquots at -80 °C.

Antibody	Concentration (mg/ml)
3A3	2.1
5G3	5.50
8E3	2
10C6.1	1.5
1E10.2	5.3

Table 2.2: Phusion PCR

Table 2.2A: PCR set-up

5X Phusion	10
10 mM dNTPs	1
10 uM FWD	2.5
10 uM REV	2.5
Template (10 ng/ μ l)	1.0
Phusion Pol.	0.5
H2O	32.5

Table 2.2B: PCR cycling conditions

Temperature (°C)	Time	No. cycles
98	2 min	1
98	1 min	35
61	1 min	
72	2 min	
72	7 min	1
4	hold	

Overlap extension

Table 2.3: Overlap extension PCR Step 1

Table 2.3A: PCR set-up

	AB fragment	CD fragment
10 X buffer	5	5
dNTPs (2.5 mM each)	4	4
Template DNA (115 ng/ μ L)	1	1
Rho1 (10 μ M)	5	-
Mutagenic primer 1 (fwd), (10 μ M)	-	5
Mutagenic primer 2 (rev), (10 μ M)	5	-
Rho2 (10 μ M)	-	5
Phusion polymerase	1	1
Water	29	29

Table 2.3B: PCR Cycling conditions

Temperature (°C)	Time	No. cycles
95	3 min	1
94	1 min	30
55	1 min	
72	2 min	
72	5 min	1
4	hold	

Table 2.4: Overlap extension PCR step 2

Table 2.4A: PCR set-up

10 X buffer	5
dNTPs (2.5 mM each)	4
Rho1 (10 uM)	5
Rho2 (10 uM)	5
AB primer (~125 ng)	~125 ng
CD primer (~125 ng)	~125 ng
Phusion polymerase	1
Water	28

Table 2.4B: PCR cycling conditions

Temperature (°C)	Time	No. cycles
95	2 min	1
94	1 min	30
55	1 min	
72	2 min	
72	7 min	1
4	hold	

Table 2.5: Peptides used in immunoprecipitation studies

Name	Amino Acid Sequence	Modification
Ac-SFKENEENIQ	SFKENEENIQ	N-terminal acetylation
IL3	SIIHTSED	None
1D4	TETSQVAPA	None
SFKE	SFKE	None
Ac-SFKE	SFKE	N-terminal acetylation
Ac-SFKA	SFKA	N-terminal acetylation
MSFKE	MSFKE	None
Ac-MSFKE	MSFKE	N-terminal acetylation

Chapter 3

3.1 Introduction

In the previous chapter, three anti-CB1 monoclonal antibodies were validated for their use in immunofluorescence. This initial validation was performed in COS-1 cells with PEI transfection. However, our qualitative observations of transfected and stained cells by immunofluorescent confocal microscopy indicated less than optimal transfection conditions. In addition to a very low transfection efficiency, many cells contained damaged, irregular, or multiple nuclei. Cells were also often misshapen with large spindle regions. To address these concerns, I tested various transfection conditions to find a more optimal protocol for observing CB1 and CB1 mutant dynamics in transiently transfected cells.

With the development, characterization, and validation of novel anti-CB1 antibodies (see Chapter 2), we now have a new tool to examine the role of the CB1 N-terminus as well as probe potential co- or post-translational modifications. One of the novel antibodies, 1E10, recognizes an epitope at the N-terminus, which raises the possibility of using this epitope as a visualization tag to assess if modifications occur (such as proteolysis of some of the N-terminus or glycosylation in or near the antibody epitope), as these would prevent binding of 1E10 to the N-terminus of the receptor. When paired with a C-terminal binding antibody, such as 1D4, it should be possible to visualize a whole-receptor population using the C-terminal binding antibody while probing for un-modified N-termini with 1E10. However, one challenge with implementing this approach in the current work is that all of the antibodies described here are mouse monoclonal antibodies, and thus would all bind the same secondary antibody. Therefore, fluorescently conjugated antibody Fabs, small antibody fragments containing the antigen-binding region, were used in a two-step labeling process for immunofluorescence.

In this chapter, optimal transfection conditions were established, a protocol to multiplex with primary antibodies from the same source animal was validated, and CB1 mutant surface expression was

visualized with confocal microscopy. Colocalization analysis of surface staining with an anti-CB1 polyclonal antibody and an intracellular anti-CB1 monoclonal antibody was used to assess the impact of N-terminal glycosylation on CB1 surface expression.

3.2 Methods

Mutants:

The primary mutants used in this chapter are shCB1-C2, CB1-GL, and SFKE-CB1. The first two mutants are described in chapter 2. The third mutant is shCB1-C2, which is a full length, minimal cysteine CB1 containing only two cysteines³⁸, into which residues SFKE were added to the N-terminus. All mutants contain the 1D4 tag at the C-terminus. Another mutant used in this work is shCB1-C2 N77Q, N83Q, which is an N-linked glycosylation deficient mutant of shCB1-C2 generated by Dr. Emily Platt.

Buffers:

Fixing buffer: 4% formaldehyde in 1X PBSSC.

Blocking buffer: 4% horse serum, 0.1% Triton-X100, 1X PBSSC.

Antibody buffer: 1X PBSSC with 0.1% Tween-20.

Immunofluorescence:

Cell lines used included HEK 293 and HEK 293 GNTI-. Several different transfection conditions were tested and are described below. Cells were seeded onto poly-L-lysine coated coverslips in 12-well plate 16 hours prior to transfection. After 36-48 hours, cells were fixed with fixing buffer and blocked with blocking buffer prior to staining. Staining conditions are also described below. After staining, coverslips were carefully transferred to glass slides with a drop of VectaShield mounting medium with DAPI and sealed with a thin layer of clear nail polish. Slides were imaged on a Zeiss Apotome 3 using the 63X oil objective. Images were processed in ImageJ.

TransfeX:

TransfeX transfection reagent was obtained from the ATCC. Several concentrations of TransfeX and DNA were tested for transfection in HEK 293 cells or HEK 293 GNTI- cells. The ratio of TransfeX to DNA was kept constant throughout.

Large T-antigen addition:

The experiments here all used the expression vector pMT4, which was originally created in the Khorana lab ⁵² as a derivative of pMT-2 ⁵³ which is a beta-lactamase derivative of p91023 ⁵⁴. As the pMT4 plasmid contains an SV40 promoter region to enable increased expression in the presence of the large T-antigen ^{55,56}, thus various concentrations of a plasmid containing large T-antigen (pRSVTag plasmid) were tested for the co-transfection of the above mutants into HEK 293 cells as discussed below. The amount of plasmid containing mutant CB1 was adjusted to keep the total DNA concentration constant.

Multiplexed immunofluorescence with rabbit polyclonal and mouse monoclonal primary antibodies:

Prior to fixing and permeabilizing, cells were incubated with rabbit polyclonal anti-CB1 (residues 1-77) antibody in antibody buffer for 5 minutes at room temperature. Then cells were fixed and permeabilized before incubating with secondary antibody (goat-anti-rabbit AF568), followed by 5G3, then goat-anti-mouse AF488 each in antibody buffer for 1 hour at room temperature.

Multiplexed immunofluorescence with mouse primary antibodies:

Multiplexed immunofluorescence was accomplished with the use of fluorescently conjugated anti-mouse Fab fragments (Jackson ImmunoResearch Laboratories Inc.). Coverslips were incubated with primary antibody in antibody buffer for 1 hour at room temperature followed by 1 hour with anti-mouse Fab fragments in the same buffer for 1 hour at room temperature. Incubation with the second primary and goat-anti-mouse AF488 proceeded in the same manner. A schematic of this workflow is presented in Figure 2.

3.3 Results

Transfection optimization: Given the issues noted in the transfections for immunofluorescence validation, optimal transient transfection conditions were explored to identify a more appropriate protocol for use in examining receptor surface expression. Specifically, several conditions were tested for Lipofectamine (not shown) and TransfeX (Figure 1). The TransfeX and DNA concentrations were increased in the transfection protocol while keeping the TransfeX:DNA ratio constant (Figure 3.1A). It appeared that the highest concentration tested, 8 uL TransfeX reagent and 4 ug DNA for transfecting a 12-well plate, performed the best. Qualitatively, the difference was marginal, and the transfection efficiency was still low. The cell line being used in these experiments, HEK 293, does not express the large T-antigen, whereas the plasmid being used, pMT4, uses an SV40 promoter^{52-54,56} that when paired with the large T-antigen can increase transfection efficiency⁵⁷. Therefore, a range of concentrations of pRSV plasmid containing large T-antigen were tested in the transfection (Figure 3.1B). The condition containing 0.4 ug large T-antigen (10% of total DNA) showed the best transfection efficiency based on qualitative observations. Several experiments in this chapter were conducted using the optimal conditions established here.

Multiplexed immunofluorescence with mouse antibodies: Another challenge in assessing CB1 subcellular localization was determination of the antibodies to use for visualization of receptor. Most mutants that had previously been generated contain the 1D4 epitope (C-terminal). Similarly, several mutants contained an N-terminal 10- or 4- residue visualization tag, developed and validated in chapter 2, which works with the 1E10 antibody. The other two antibodies characterized and validated in Chapter 2, 3A3 and 5G3, recognize an epitope within the intracellular loop 3 region of CB1. While all these antibodies are useful in visualizing CB1 in immunofluorescence, multiplexing with these antibodies is a challenge as they are all derived from mice. To evaluate the subcellular localization of various CB1 isoforms, multiplexing with these previously validated antibodies was accomplished with the use of

fluorescently conjugated anti-mouse Fabs. A schematic of the 4-step labeling technique is shown in Figure 3.2A. Validation of the technique involved staining both a negative control mutant, shCB1-C2, which is not recognized by 1E10, and SFKE-CB1, which is recognized by both (Figure 3.2B). Multiplexed staining of shCB1-C2 showed that staining with the fluorescently conjugated Fabs after the first primary antibody prevented staining with the fluorescently conjugated secondary antibody (goat-anti-mouse AF488) regardless of which primary antibody was used first.

Subcellular localization of CB1: This technique was then used to explore whether the CB1 N-terminus affects the subcellular localization of CB1. Tagged CB1 (SFKE-CB1) and CB1-GL, an N-terminal truncation mutant, were transiently transfected in HEK cells and probed using 1E10 (N-terminal) and 1D4 (C-terminal) primary antibodies (Figure 3.3). Some cells appeared to show a slight increase in intracellular staining with 1D4 compared to N-terminal staining with 1E10 (Figure 3.3, top). This could potentially indicate that the population at the cell surface lacks the full CB1 N-terminus as it is not recognized by the n-terminal antibody, 1E10. However, this trend was only seen in some cells, while others contained a similar distribution of staining across the two antibodies (Figure 3.3, bottom). Given the divergence in results across data collected, the experiment was repeated with both the N-terminally truncated CB1-GL (Figure 3.4A) and the SFKE-tagged full length receptor (Figure 3.4B). CB1 distribution in both samples remained heterogeneous, and further analysis was not pursued. Overall, it remains unclear whether the CB1 N-terminus is cleaved or if a subpopulation of CB1 lacks the full N-terminus. The heterogeneous state of CB1 expression in transient transfection further obscures potential subtle regulatory trends. Further work to assess the population and distribution of CB1 in cells is required and would benefit from the generation of stable cell lines or endogenous sources.

CB1 N-terminal glycosylation: Finally, N-terminal glycosylation was evaluated for its role in CB1 surface expression. Glycosylation-deficient CB1 mutant shCB1-C2 N77Q, N83Q was previously developed by Dr. Emily Platt and was shown to lack N-linked glycosylation by PNGase F digest. Previous live cell

imaging of shCB1-C2 and its glycosylation deficient mutant in HEK 293 cells by Dr. Emily Platt showed a decrease in surface expression of CB1 in the glycosylation deficient mutant (Appendix 3). This work was replicated successfully in the same cell line in the present work (Figure 3.5). This decreased surface staining could indicate that N-linked glycosylation plays a role in CB1 surface expression, but further analysis is necessary to support this finding.

Impact of glycosylation on CB1 surface expression: shCB1-C2 and the glycosylation-deficient mutant were transiently expressed in HEK 293 cells and probed with a rabbit polyclonal antibody that recognizes the first 77 residues of CB1 or 5G3, which recognizes an intracellular epitope. Colocalization analysis was conducted to evaluate the overlap in staining and assess whether glycosylation of the CB1 N-terminus influenced CB1 surface expression (Figure 3.6). The imaging and colocalization analysis again revealed a great deal of heterogeneity in the expression and/or staining protocol. From this data, it remains unclear how cleavage or N-linked glycosylation plays a role in regulating CB1 surface expression.

3.4 Discussion

Optimal transient transfection conditions were established to maximize transfection efficiency and workflow. TransfeX transfection reagent was obtained from the ATCC, and optimal transfection conditions were determined for both the concentration of TransfeX and DNA as well as the concentration of plasmid containing large T-antigen. These optimized conditions increased the overall transfection efficiency and allowed for analysis of more transfected cells in fewer images. The best transfection occurred around the edges of cell clusters, so transfection efficiency was also improved by transfecting when cells were sub-confluent (50-70% confluent) to maximize these higher efficiency zones.

Most of the antibodies used in this chapter were generated from mice, so a method was established to multiplex with mouse monoclonal antibodies of similar or unknown Ig subtype. This method was validated to ensure that there was sufficient signal from the Fabs bound to the first primary

antibody and that there was minimal crosstalk between the first primary and secondary antibody or the second primary antibody and the Fabs.

N-linked glycosylation of CB1 was established and N-linked glycosylation sites were mutated previously by Dr. Emily Platt. Preliminary live cell IF results were replicated successfully using rabbit polyclonal antibodies to surface-stain live cells. To further probe the impact of N-linked glycosylation on CB1 surface expression, an N-terminal binding antibody (rabbit anti-CB1, residues 1-77) and an intracellular binding antibody, 5G3, were used to probe surface expression of a full-length mutant CB1 and a full-length, glycosylation deficient CB1. Colocalization analysis was performed to assess the surface expression of CB1 relative to the total CB1 population, but expression in both samples was very heterogeneous. This is likely due to the transient transfection system, which often results in a high degree of heterogeneity. Future experiments would benefit from generation of stable cell lines or endogenous expression systems to remove some of the heterogeneity problem. Overall, mutation of N-linked glycosylation sites did not appear to have a large impact on CB1 surface expression in transiently transfected HEK cells.

3.5 Figures

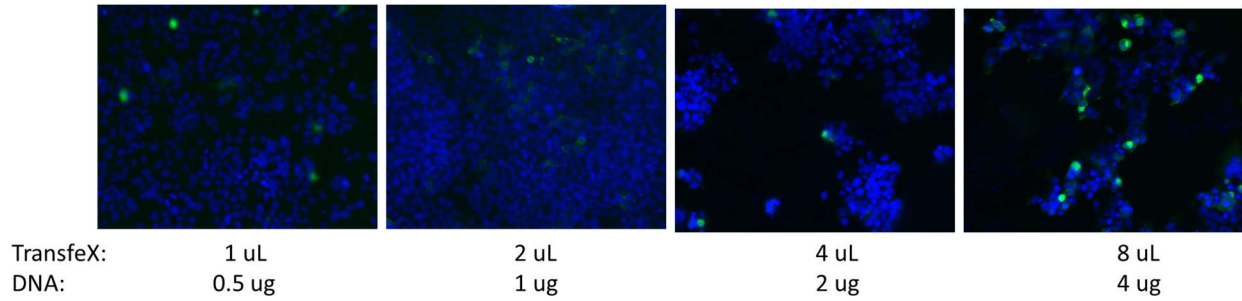


Figure 3.1A: Various concentrations of TransfeX and DNA were tested in the transfection of SFKE-CB1-C2 in HEK 293 cells. SFKE-CB1-C2 was transiently transfected into HEK 293 cells with TransfeX transfection reagent. Various concentrations were tested, maintaining a TransfeX to DNA ratio of 2:1. Cells were stained with 1D4 and a goat-anti-mouse AF488 secondary antibody. Confocal images were collected on a Zeiss Apotome 3 confocal microscope at 63X magnification.

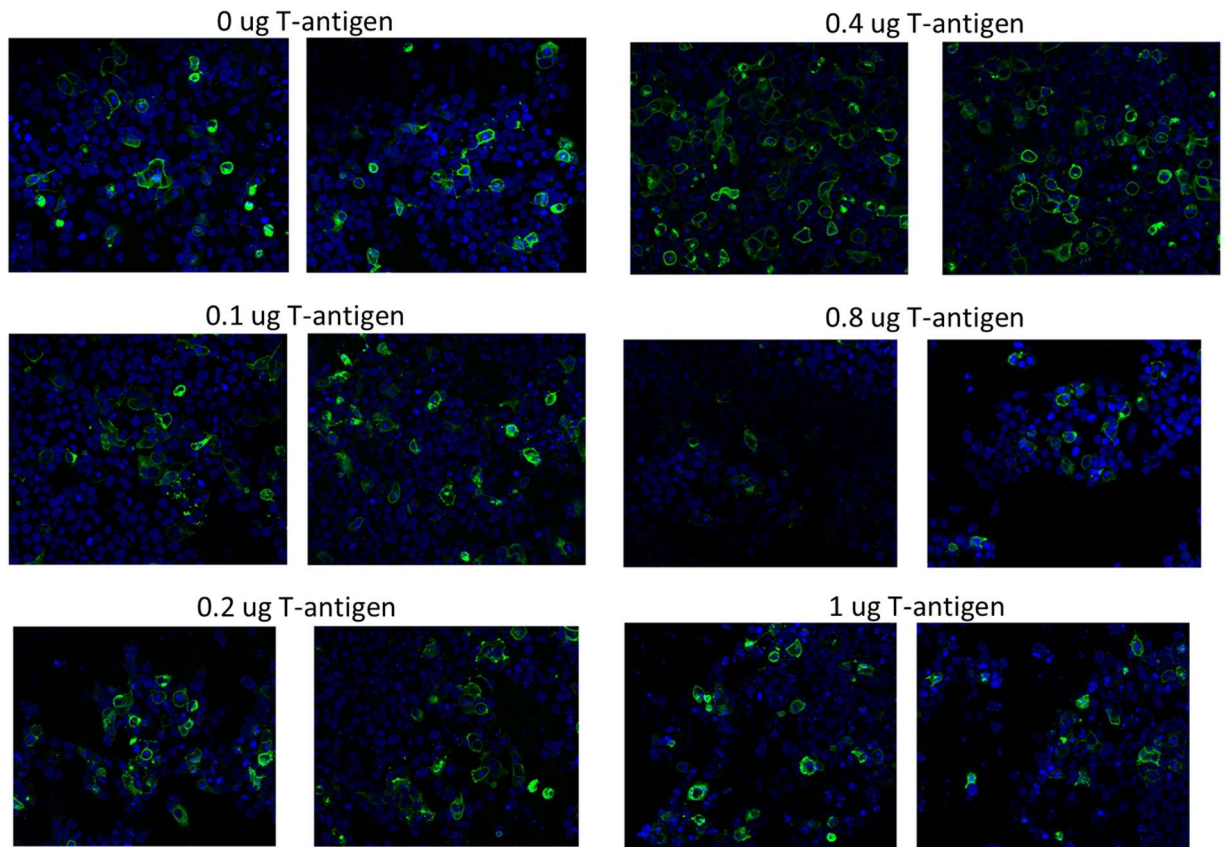


Figure 3.1B: Various concentrations of large T-antigen plasmid were tested in the transfection of both HEK 293 cells with SFKE-CB1-C2. SFKE-CB1-C2 was transiently transfected into HEK 293 cells with TransfeX transfection reagent. Total DNA was maintained at 4 ug. Cells were stained with 1E10 and a goat-anti-mouse AF488 secondary antibody. Confocal images were collected on a Zeiss Apotome 3 confocal microscope at 63X magnification.

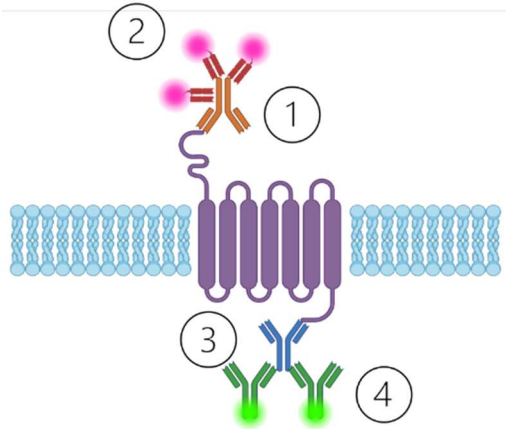


Figure 3.2A: Schematic of multiplexed immunofluorescence with fluorescently conjugated Fabs. After fixing, blocking, and permeabilizing, samples were incubated with the first primary antibody (1). Samples were then incubated with fluorescently conjugated (AF594) anti-mouse Fabs (2). After incubation with the second primary antibody (3), samples were incubated with the secondary antibody, goat-anti-mouse AF488 (4).

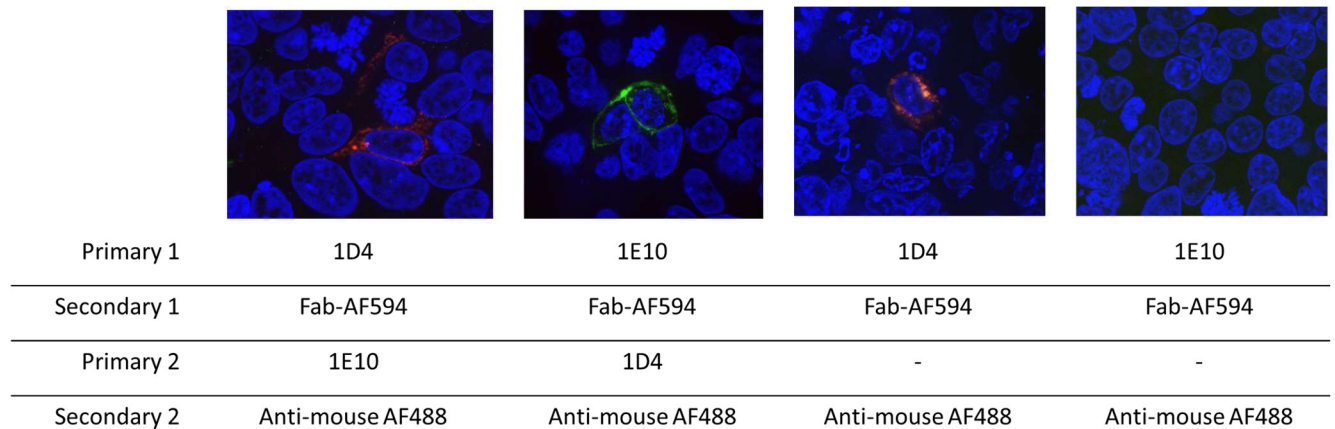


Figure 3.2B: Validation of technique (IF images including controls). HEK 293 cells were transfected with shCB1-C2 (C-terminally tagged with 1D4, full-length mutant). Various combinations of primary and secondary antibodies were tested to identify potential off-target interactions. Confocal images were collected on a Zeiss Apotome 3 confocal microscope at 63X magnification.

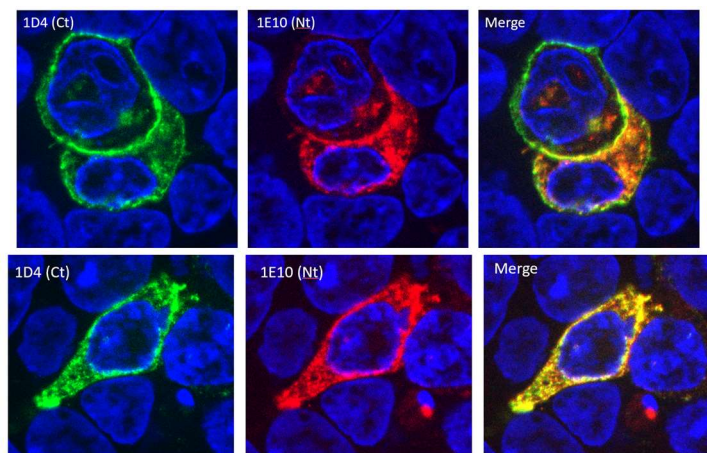


Figure 3.3: Confocal images of HEK cells transiently transfected with SFKE-CB1-C2. SFKE-CB1-C2 was transiently transfected into HEK 293 cells and stained according to the scheme in Figure 3.2A with 1E10 as the first primary antibody and 1D4 as the second primary antibody. Confocal images were collected on a Zeiss Apotome 3 confocal microscope at 63X magnification.

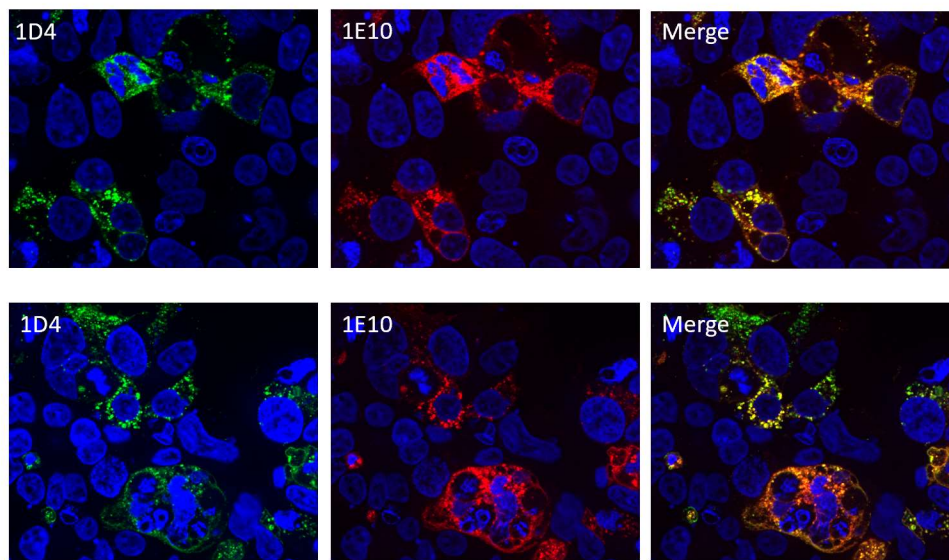


Figure 3.4A: Immunofluorescence of CB1 N-terminal truncation mutant, CB1-GL. CB1-GL was transiently transfected into HEK 293 cells and stained according to the scheme in Figure 3.2A with 1E10 as the first primary antibody and 1D4 as the second primary antibody. Confocal images were collected on a Zeiss Apotome 3 confocal microscope at 63X magnification.

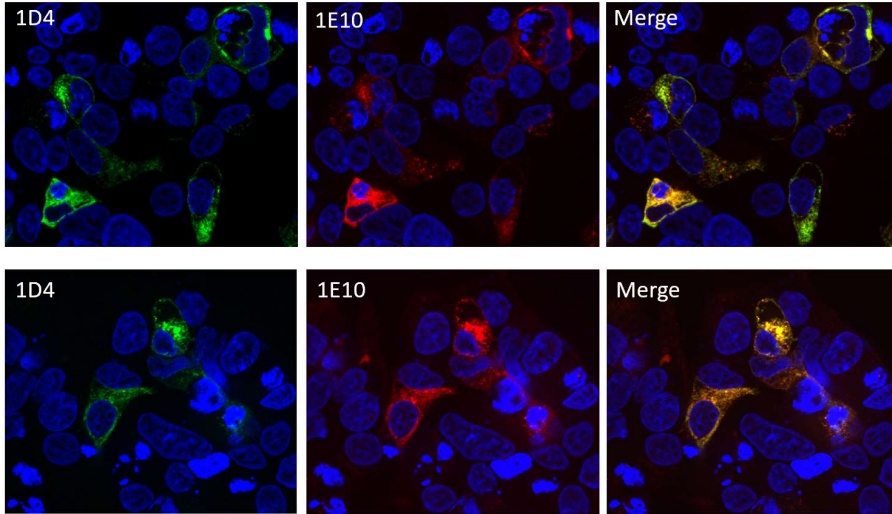


Figure 3.4B: Immunofluorescence of tagged, full-length receptor, SFKE-CB1-C2. SFKE-CB1-C2 was transiently transfected into HEK 293 cells and stained according to the scheme in Figure 3.2A with 1E10 as the first primary antibody and 1D4 as the second primary antibody. Confocal images were collected on a Zeiss Apotome 3 confocal microscope at 63X magnification.

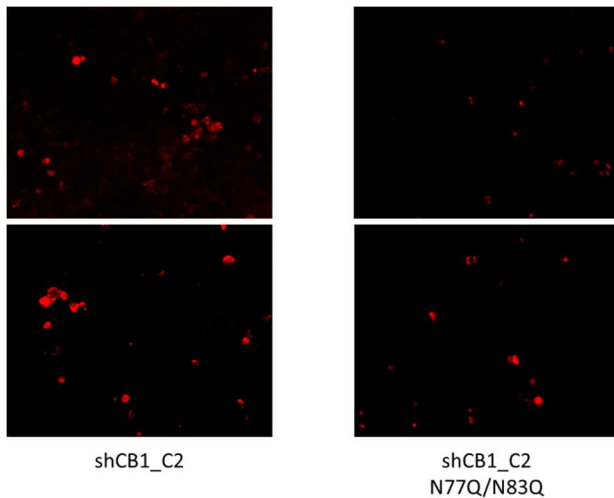


Figure 3.5: Live cell staining of surface receptor. shCB1-C2 or glycosylation knock-out mutant shCB1-C2 N77Q, N83Q were transfected into HEK 293 GNTI- cells, then stained with rabbit polyclonal (residues 1-77) and goat-anti-rabbit AF568 in 1X PBSSC. Images of live cells in 1X PBSSC were captured on a Nikon Eclipse Ti2 at 20X magnification.

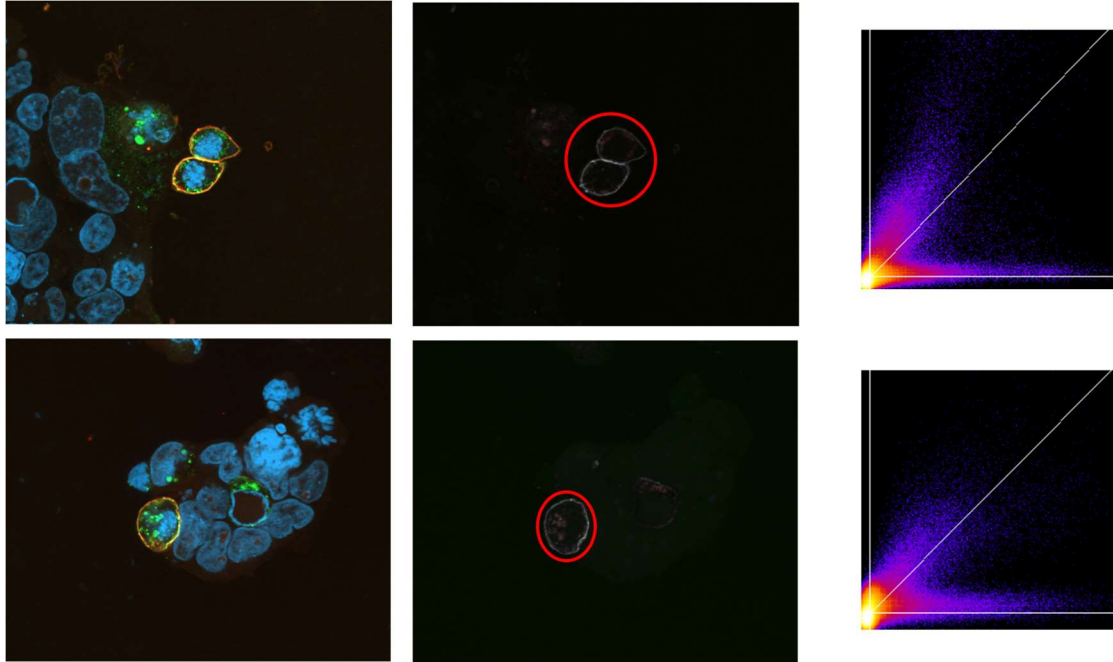


Figure 3.6A: Immunofluorescence of shCB1-C2 with colocalization analysis. CB1-C2 was transiently transfected into HEK 293 cells and stained with rabbit-anti-CB1 polyclonal antibodies (extracellular) prior to fixing and permeabilizing, then stained with 5G3 (intracellular antibody). Confocal images were collected on a Zeiss Apotome 3 confocal microscope at 63X magnification. Left image shows all channels merged. Center image shows the red and green channels overlapped with a representative region of interest (ROI). Right image shows scatterplot of pixel intensity.

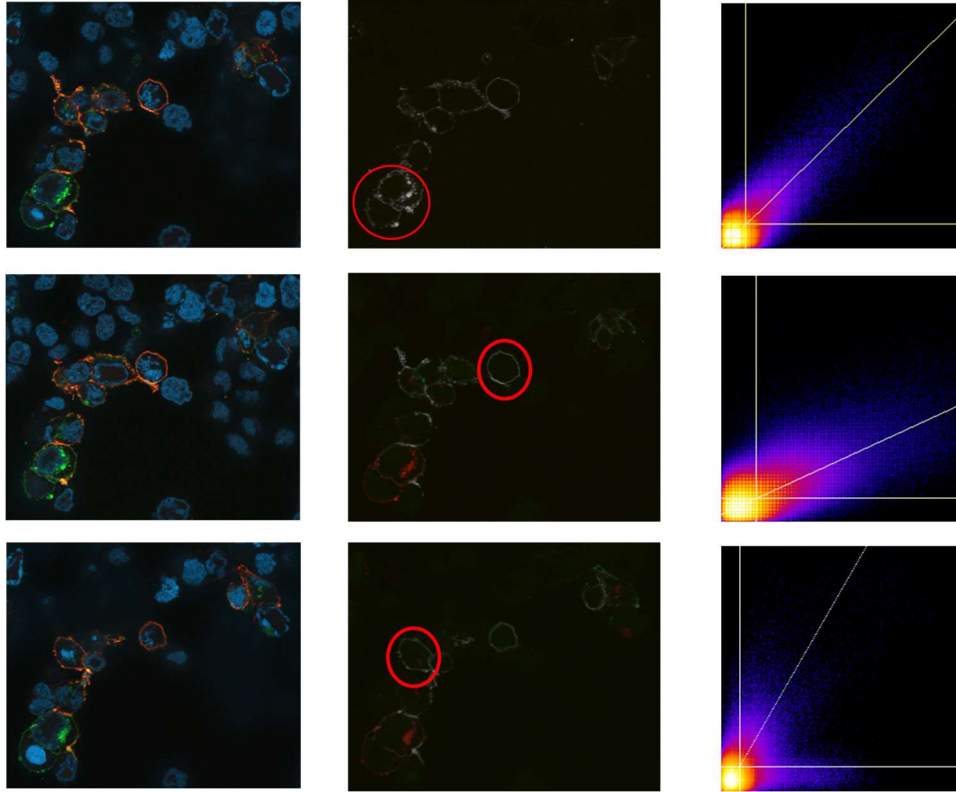


Figure 3.6B: Immunofluorescence of shCB1-C2 N77Q, N83Q with colocalization analysis. CB1-C2 N77Q, N83Q was transiently transfected into HEK 293 cells and stained with rabbit-anti-CB1 polyclonal antibodies (extracellular) prior to fixing and permeabilizing, then stained with 5G3 (intracellular antibody). Confocal images were collected on a Zeiss Apotome 3 confocal microscope at 63X magnification. Left image shows all channels merged. Center image shows the red and green channels overlapped with a representative ROI. Right image shows scatterplot of pixel intensity.

3.6 Tables

Table 3.1: Colocalization analysis summary for shCB1-C2

Figure	R total	m	b	R colocalization
5A (top)	0.472	1.042	17.8	0.4903
5A (bottom)	0.443	1.007	23.8	0.4844

Table 3.2: Colocalization analysis summary for shCB1-C2 N77Q, N83Q

Figure	Rtotal	m	b	R colocalization
5B (top)	0.282	1.644	-13	0.4592
5B (middle)	0.560	0.458	14	0.5780
5B (bottom)	0.239	1.736	-15.1	0.4723

Chapter 4

4.1 Introduction

Immunoaffinity purification is a common method for purification of both endogenous and recombinant protein. Protein purification is an important tool in any biochemical or molecular biological toolbox, with success typically measured by the concentration and purity of the eluate. This can be evaluated using SDS-PAGE, Western blots, SEC spectra, unique spectral or functional features of the desired protein, and more ⁵⁸⁻⁶⁰.

Several factors contribute to a successful purification. These include increasing the efficiency of binding and elution, as these are key for increasing the concentration of the eluate and increasing the effective and specific binding to increase the purity of the final product.

Protein purification can exploit different protein characteristics including size, charge, and affinity ⁵⁹⁻⁶². Affinity purification is one of the more common methods used. In the case of recombinant protein, various tags can be introduced to enable the protein to bind to purification columns or to track the protein during the purification process ^{60,63}. When the protein source is endogenous and/or a wild-type protein, elements or characteristics of the protein itself must be used. This requires a level of understanding of the protein of interest at the beginning of the purification process or previously designed tools or affinity reagents to pull-down the protein of interest. Many affinity purification techniques, while specific for the protein of interest, are not specific for functional protein or folded protein.

1E10 antibody may be a useful tool for purifying tagged receptors. In chapter 2, 1E10 was validated for use in visualization and immunoprecipitation. Immunoaffinity purification is similar to immunoprecipitation as both methods employ an antibody to exclude a specific target from a mixed solution. For the purposes of this work, the primary distinctions between the two are the scale, column, and elution method. In these studies, immunoprecipitation volumes are kept constant and small while in

immunoaffinity purification these can be scaled up and down more easily. Immunoprecipitation employed antibody binding to pre-coupled protein-A Sepharose columns while antibodies were coupled directly to Sepharose columns for immunoaffinity purification. Finally, in immunoprecipitation studies, samples were eluted by denaturing the antibodies and receptor in gel-running buffer with DDT. For immunoaffinity purification, peptide corresponding to the antibody epitope is used to competitively displace the receptors off the antibody column. Given the success of 1E10 in immunoprecipitation in Chapter 2, I sought to test its potential use in immunoaffinity purification, since both techniques rely on the affinity of the antibody for the target. In this chapter, I tested this idea. I used 10- and 4-residue tags corresponding to the 1E10 epitope introduced to the N-terminus of various CB1 and rhodopsin constructs and tested their ability to be purified using 1E10 immunoaffinity purification. For a positive control, 1D4 antibody was also tested, as all constructs contain the 1D4 epitope and 1D4 is a well-established tool for immunoaffinity purification (noted below).

1D4 and Flag are common purification tags. Two commonly used purification tags consist of epitopes for the 1D4 and Flag antibodies. The 1D4 epitope is found endogenously at the C-terminus of many opsins⁶⁴ and has been well validated for purification of both endogenous and tagged recombinant protein. The 1D4 epitope can also be introduced to other, non-opsin proteins. The “Flag tag” is a synthetic sequence designed to be distinct from endogenous protein sequences⁶⁵. The Flag tag can only be used with recombinant protein as the sequence must be added to protein constructs prior to expression.

Multivalent peptides may improve immunoaffinity purification. One way to increase the efficiency of elution for affinity chromatography is through use of multivalent ligands⁶⁶. In the case of immunoaffinity purification, this involves the use of multivalent peptides, which contain multiple epitopes linked together, thus increasing the local concentration of the antibody epitope which can lead to more efficient elution in immunoaffinity purification. The Flag tag takes advantage of this principle in

the 3xFlag tag⁶⁷, which contains three versions of the epitope. In this chapter, I tested the application of this principle using multivalent peptides to elute from 1D4 and 1E10 immunoaffinity columns.

4.2 Methods

Peptides: All peptides were obtained from GenScript. Peptides, sequences, modifications, and purity are noted in Table 4.1.

Buffers:

Buffer A: 1mM HCl pH 2.8.

Buffer B: 0.1M NaHCO₃, 500mM NaCl pH 8.3

Buffer C: 0.2M Glycine pH 8.0

Buffer D: 0.1M acetic acid/NaCH₃COO, 500mM NaCl pH 4.0

Buffer E: 0.1M Tris-HCl, 500mM NaCl pH 8.0

Buffer F: PBSSC + 0.004% sodium azide

Buffer G: 1X PBSSC, 0.05% DDM

Buffer H: 5 mM MES, 0.05% DDM pH 6.0

1E10 coupling to CNBr activated Sepharose: 1.5 g CNBr Sepharose (GE Healthcare) was resuspended in 5 mL buffer A and nutated for 30 minutes at room temperature, then washed with 300 mL Buffer A over approximately 30 minutes. Then beads were washed in 5 mL buffer B before addition of antibodies. 5 mL of 5 mg/mL antibody was added to the activated column and nutated for 1 hour at room temperature, then overnight at 4 °C. Flow-through from column was collected before washing with 25 mL buffer B. The buffer was exchanged for buffer C by running 10 mL buffer C through the column, then beads were nutated for 2 hours at room temperature in 5 mL buffer C. Beads were then washed with 5 cycles of 25 mL buffer D followed by 25 mL buffer E. Buffer was exchanged for buffer F and beads were stored in 5 mL buffer F (~50/50 slurry).

Protein expression: Transient transfection in COS-1 cells and harvest were conducted as described in Chapter 2. Cell pellets were resuspended in 0.9 mL buffer per 150 mm tissue culture plate transfected. Membranes were solubilized in either RIPA or 1X PBSSC + 1% dodecylmaltocyclide (DDM) with protease inhibitors (1X HALT, 5 µg/mL Leupeptin, 0.5 mM PMSF). After pelleting at either 14,000 rpm in a table-top ultracentrifuge for 20 minutes or at 40,000 rpm for 30 minutes in a TI-60 rotor, supernatant was collected, and total protein concentration was measured using the Lowry Assay (BioRad).

Immunoaffinity purification: All rhodopsin constructs were incubated for at least 1 hour at room temperature with 5-10 µM 11-cis retinal in the dark to reconstitute protein. For these constructs, purifications were conducted in the dark under red lights.

For small-scale purification, 50 µg total protein (in solubilized membranes) was added to 100 µL solubilization buffer. Then 25 µL of 50/50 antibody-sepharose slurry was added and all were nutated 90 minutes at 4 °C. Supernatant was collected before washing three times with 150 µL solubilization buffer with a 15-minute nutation at 4 °C per wash. After washing, receptor was eluted in 20 µL Elution buffer (solubilization buffer + 200 µM peptide), incubating 30 minutes at room temperature per elution. For denature samples, 25 µL gel running buffer was added to columns, then incubated for 30 minutes at either 65 °C for CB1 mutants or room temperature for rhodopsin mutants.

For large-scale purification, 500 µL 50/50 antibody-bead slurry was added to solubilized membranes, volume and concentrations were adjusted to 15 mL 1 M NaCl, 2 mM MgCl₂, 1% DDM, 1X PBSSC, then nutated overnight at 4 °C. After collection of flow-through, columns were washed with 30 mL Buffer G, then 30 mL Buffer H. Receptor was eluted in 200 µL Buffer H + 40 mM NaCl, 200 µM corresponding peptide.

After purification, 25 µL each sample in 1X gel running buffer were applied to 8% acrylamide gels. The gels were run at 50-75 V until dye began running off the gel. For Coomassie staining, gels were first rinsed with water for 20 minutes, then incubated for 1 hour in Instant Blue (Abcam). For Western

Blots, gels were transferred to PVDF membranes for 1 hour at 190 mA. Membranes were blocked overnight in 50% Licor blocking solution, then stained with 1D4 primary antibody and goat-anti-mouse AF680 secondary antibody. Membranes were visualized on Sapphire Imager, images were processed with ImageJ, and labels added in Inkscape.

4.3 Results

1E10 can be used to purify CB1-GL. Given the success of 1E10 for use in immunoblot, immunoprecipitation, and immunofluorescence (Chapter 2), it was also tested for use in immunoaffinity purification. 1E10 was coupled to CNBr activated Sepharose, then used to purify CB1-GL, a CB1 mutant against which 1E10 was originally generated (Figure 4.1). Overall, this purification was successful, with CB1-GL strongly present in each of the three elution lanes. However, a substantial amount of receptor remained on the column, as indicated by a strong band at ~30 kDa in the denatured lane. Overall, these purification results are consistent with purification of the same construct with 1D4-coupled beads (Figure 4.1), indicating that 1E10 may be useful for immunoaffinity purification.

Detergent conditions alter immunoaffinity purification of CB1-GL for both antibodies. Given the previous ability to immunoaffinity purify CB1-GL solubilized in RIPA, the same protocol was then tested with DDM (dodecylmaltoside), a commonly used detergent used in GPCR studies. In this case, DDM did not appear to improve overall purification with the intensity of elution bands appearing to decrease while the ~30 kDa band in the denature lane remains high intensity (Figure 4.2). DDM is a gentler detergent than those used in RIPA buffer, so this result was surprising. The high intensity of the ~30 kDa band in the denature lane indicates that most of the receptor remained on the column after elutions, which could indicate a stronger antibody-antigen interaction with DDM. It is possible that harsher detergent conditions weaken the binding interaction between 1E10 and the epitope, allowing for more efficient elution due to a less stable receptor or interaction. This demonstrates the importance of

choosing detergent and buffer conditions that work well for both the protein of interest and antibody being used in immunoaffinity purification.

Modifications of the 1E10 epitope can be used to alter antibody affinity and improve purification of CB1-GL by 1E10. One of the advantages of using the 1D4 antibody for purification schemes lies in its intermediate affinity for the epitope ($\sim 1 \mu\text{M}$), which makes it possible to release the bound antibody using competing peptides⁶⁴. Based on the peptide competition assays from Chapter 2, 1E10 seems to have a higher affinity for its epitope, which would be a disadvantage in immunoaffinity purification as it can make it difficult to elute protein from the column. A single glycine addition to the extreme N-terminus of CB1-GL can decrease the affinity of 1E10 for the receptor (Figure 4.3A), as does mutating K90 and E91 to alanine (Figure 4.3A). Both mutants were tested for immunoaffinity purification with 1E10 to assess if these epitope-alterations could potentially improve the elution yield from the column and generate a more efficient purification tag. The single glycine addition mutant did appear to perform slightly better than CB1-GL in immunoaffinity purification by 1E10, as evidenced by the strong band at ~ 30 kDa in the first elution lane (E1) and a reduction in the intensity of the same band in the denatured lane (Figure 4.3B, top left). In contrast, the double alanine mutant did not purify well with either 1E10 or 1D4 immunoaffinity purification as evidenced by only faint banding in the elution lanes and a strong band in the flow-through lane of the 1D4-purification (Figure 4.3B, bottom). Given the lack of improvement with alanine mutations, it would appear this sequence would not be a good candidate for a purification tag. To further probe the use of the single glycine addition epitope sequence for use with 1E10, this purification was repeated with PBSSC/DDM buffer rather than RIPA buffer (Figure 4.3C). Results of this purification were consistent, showing overall improvement compared to CB1-GL. Given the preliminary success of the single glycine addition, this sequence, GSFKENEENIQ, presents a potential purification tag for use with 1E10. Of note, this tag would include acetylation of the terminal glycine residue, rather than the serine.

1E10 can be used to purify tagged rhodopsin mutants but is not as effective as 1D4. Either a 4- (SFKE) or 10-residue (SFKENEENIQ) tag was added to the N-terminus of a synthetic human rhodopsin mutant. Given the tag is included in the expressed receptor, it is expected that N-terminal processing would proceed in the same manner as with CB1_GL, including cleavage of the start methionine and acetylation of the terminal serine residue. These mutants were then purified with 1E10 or 1D4 as described previously. In small-scale purification, both antibodies appeared to purify tagged receptor similarly (Figure 4.4A), however, when scaled up to a 0.5 mL column volume, 1D4 outperformed 1E10 (Figure 4.4B), with most of the protein coming off in the last elution. No denature condition was evaluated for the large columns so that beads could be regenerated for re-use. Of note, the scaled-up purification used PBSSC + DDM, whereas the smaller-scale purifications used RIPA buffer. This result again indicates the importance of using the appropriate buffer conditions for purification.

Multivalent peptides improve elution from 1D4 immunoaffinity column slightly, but do not improve elution from 1E10 immunoaffinity column. While optimizing the antibody-tag affinities can improve immunoaffinity purification, another potential way to improve immunoaffinity purification is by optimization of the eluting agent, in this case, the competing peptide. A classic example is the Flag tag⁶⁷. To improve the efficacy of the eluting peptide, multivalent peptides were developed for both 1D4 and 1E10 columns. Both peptides contain two copies of the epitope, connected by a short linking region. For 1D4, the connector region is two glutamate residues as this was shown to work for an internal epitope region on a previous construct⁶⁸, making the final multivalent peptide TETSQVAPAEETETSQVAPA. For 1E10, a series of 4 glycine residues was used as a connector region given the ability of 1E10 to recognize the epitope with a single glycine residue addition at the N-terminus, making the final multivalent peptide SFKEGGGGSFKE. While elution of rhodopsin from ROS was improved by the multivalent peptide in elution 2 (Figure 4.5A, E2), elution from the 1E10 column was not improved by the multivalent peptide

(Figure 4.5B). Overall, multivalent peptides did not increase elution efficiency dramatically for either antibody.

4.4 Discussion

Overall, 1E10 was able to purify mutant CB1 and tagged rhodopsin. While small-scale purification of tagged rhodopsin mutants showed similar efficacy between the two antibodies, this was not maintained when the purifications were scaled up. Purification was improved by introducing a single glycine mutation at the start of the 1E10 epitope, which reduces the affinity of the antibody. However, alanine mutations that also lower affinity did not improve purifications. Thus, a purification tag with a glycine at the start could improve functionality at increased column sizes.

In retrospect, the minimal improvement provided by the multi-valent elution peptides for 1E10 and 1D4 is not surprising. Placement preference of both 1D4 and 1E10 may hinder the ability of multivalent peptides to improve purification. The 1D4 antibody requires the epitope be located at the extreme C-terminus, and thus has very poor recognition of internal epitopes^{48,69}. Similarly, as discussed in Chapter 2, 1E10 must be located at the extreme N-terminus for optimal antibody binding due to the inclusion of the N-terminal acetyl group in the antibody epitope. However, other multi-valent techniques could still potentially improve purifications using antibody. For example, branching the epitope peptides so they all present in the preferred orientation could improve elution.

4.5 Figures

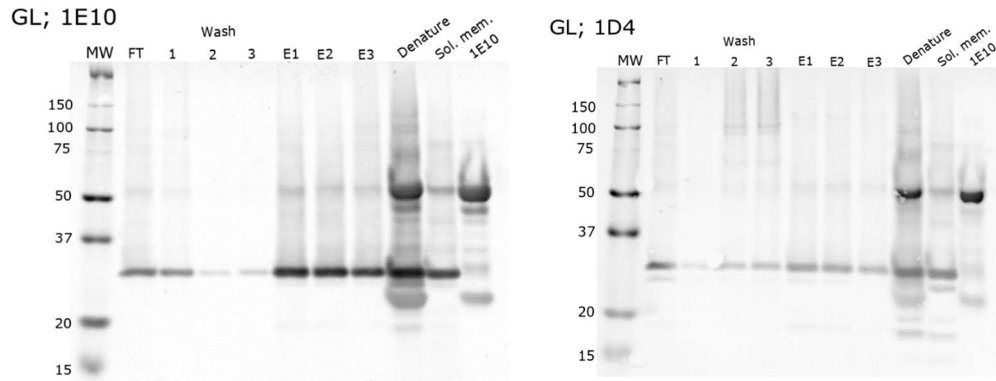


Figure 4.1: Purification of CB1-GL with 1E10 and 1D4 in RIPA. CB1-GL was purified with either 1E10- or 1D4-coupled sepharose as indicated. Solubilization, wash, and elution buffer were all 1X RIPA. Elution buffer also contained 200 μ M peptide, N-terminally acetylated SFKENEENIQ for 1E10 and TETSQVAPA for 1D4. After three elutions (E1, E2, and E3), remaining protein was denatured off sepharose beads in gel loading buffer at 65 °C for 30 minutes. Western blots were stained with 1D4 primary antibody and goat-anti-mouse AF680 secondary. Of note, bands at ~50 kDa and ~25 kDa in the denatured lane represent heavy and light antibody chains (compare with the 1E10 alone lane).

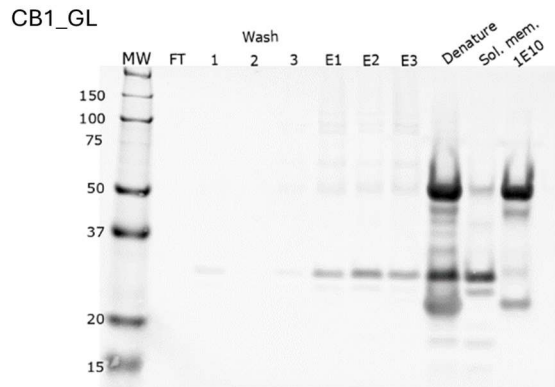


Figure 4.2: Purification of CB1-GL with 1E10 in PBSSC + 1% DDM. CB1-GL was purified with either 1E10-coupled sepharose. Solubilization, wash, and elution buffer were all 1X PBSSC + 1% DDM. Elution buffer also contained 200 μ M N-terminally acetylated SFKENEENIQ. After three elutions (E1, E2, and E3), remaining protein was denatured off sepharose beads in gel loading buffer at 65 °C for 30 minutes. Western blots were stained with 1D4 primary antibody and goat-anti-mouse AF680 secondary. Of note, bands at ~50 kDa and ~25 kDa in the denature and 1E10 lane represent heavy and light antibody chains.

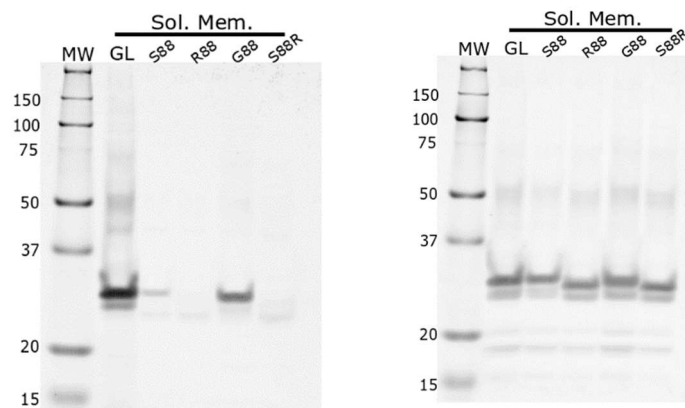


Figure 4.3A: Mutations in the N-terminus of CB1-GL decrease the affinity of 1E10 for the receptor. Mutant CB1 was transiently expressed in Cos-1 cells. Western blots of RIPA solubilized membranes were probed with 1E10 (left) or 1D4 (right, expression control).

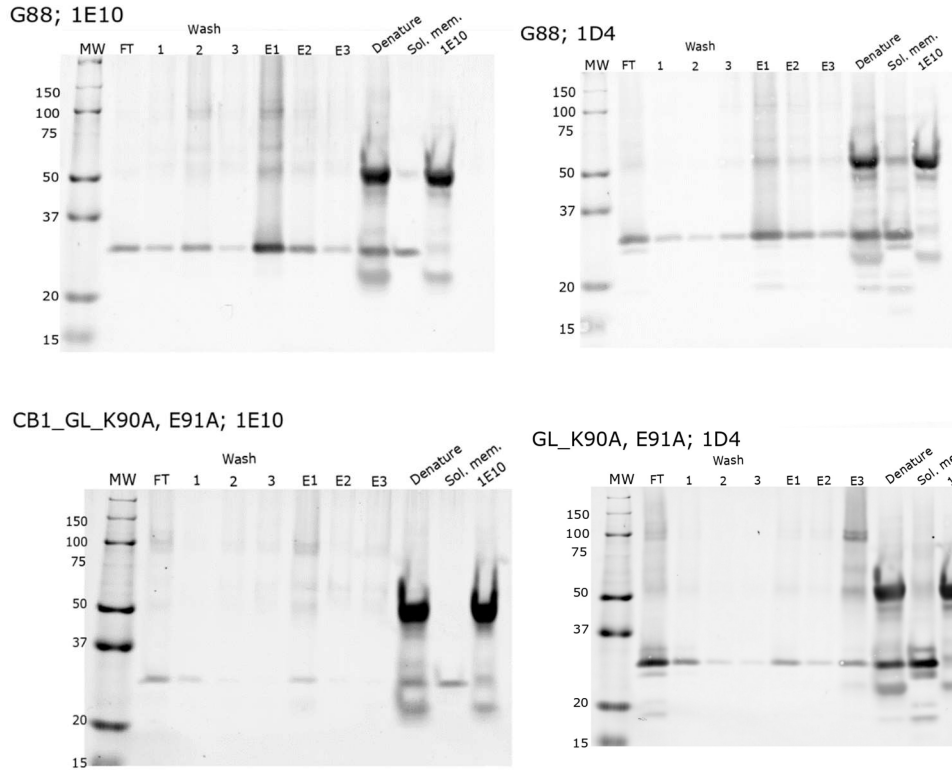


Figure 4.3B: Purification of CB1-GL N-terminal mutants with 1E10 or 1D4. CB1-GL G88 or CB1-GL K90A, E91A were purified with either 1E10- or 1D4-coupled sepharose as indicated in RIPA. After three elutions (E1, E2, and E3), remaining protein was denatured off sepharose beads in gel loading buffer at 65 °C for 30 minutes. Western blots were stained with 1D4 primary antibody and goat-anti-mouse AF680 secondary.

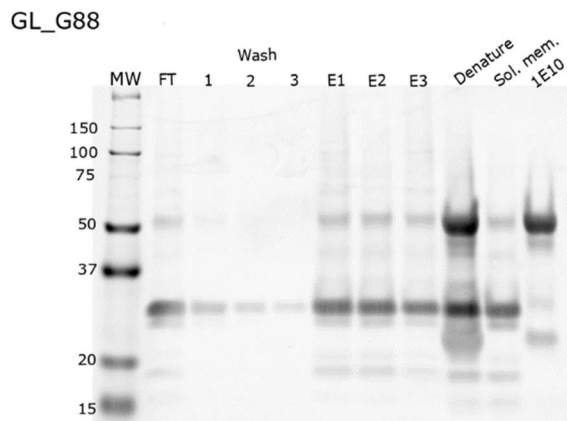


Figure 4.3C: Immunoaffinity purification of CB1-GL G88 with 1E10 in PBSSC + DDM. CB1-GL G88 was purified with either 1E10- coupled sepharose. Solubilization, wash, and elution buffer were all 1X PBSSC + 1% DDM. Elution buffer also contained 200 μ M N-terminally acetylated SFKENEENIQ. After three elutions (E1, E2, and E3), remaining protein was denatured off sepharose beads in gel loading buffer at 65 °C for 30 minutes. Western blots were stained with 1D4 primary antibody and goat-anti-mouse AF680 secondary. Of note, bands at ~50 kDa and ~25 kDa in the denature and 1E10 lane represent heavy and light antibody chains.

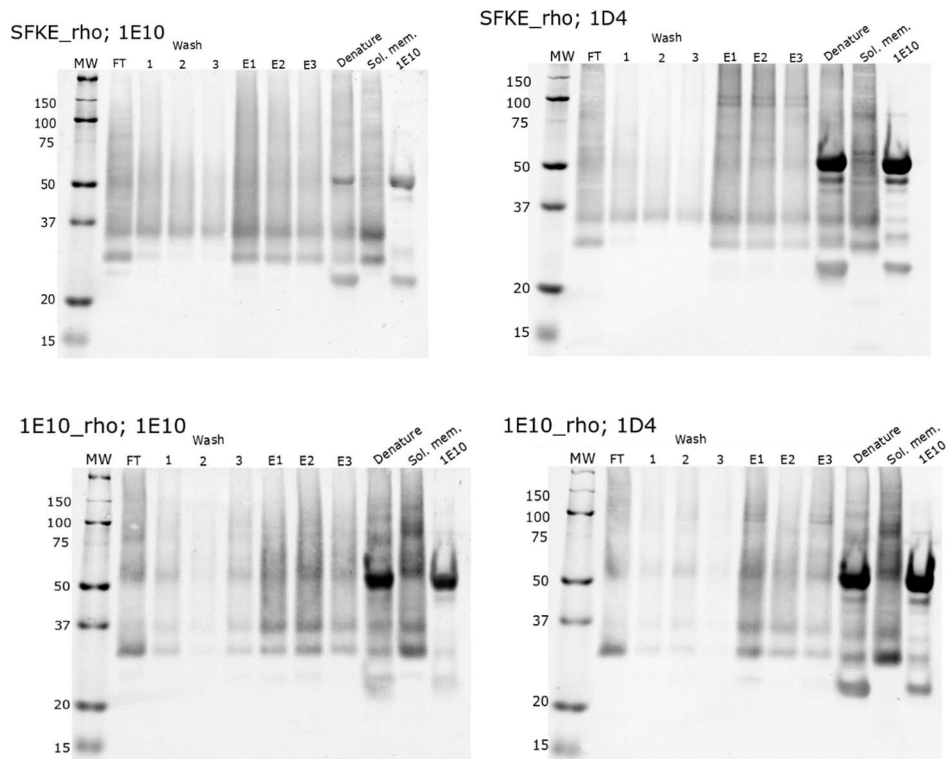


Figure 4.4A: Purification of tagged rhodopsin mutants with 1E10 or 1D4. SFKE- or SFKENEENIQ-tagged rhodopsin were purified with either 1E10- or 1D4-coupled sepharose as indicated in RIPA. After three elutions (E1, E2, and E3), remaining protein was denatured off the sepharose beads in gel loading buffer at 65 °C for 30 minutes. Western blots were stained with 1D4 primary antibody and goat-anti-mouse AF680 secondary.

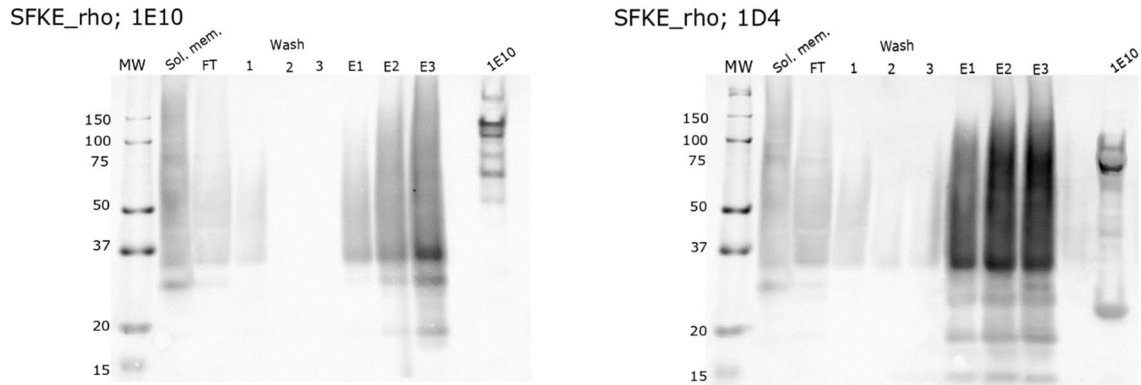


Figure 4.4B: Large-scale purification of tagged rhodopsin. SFKE-tagged rhodopsin was solubilized in 1X PBSSC + 1% DDM, then purified with 0.5 mL column of either 1E10- or 1D4-coupled sepharose as indicated. Both Western blots were stained with 1D4 primary antibody and goat-anti-mouse AF680 secondary.

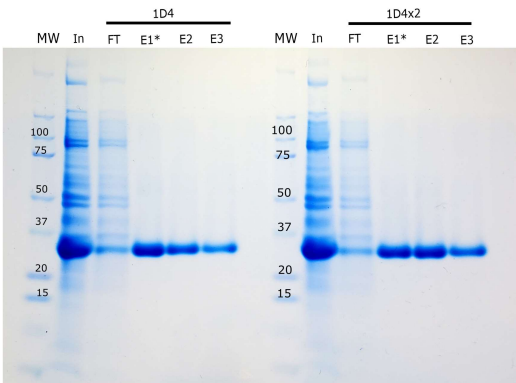
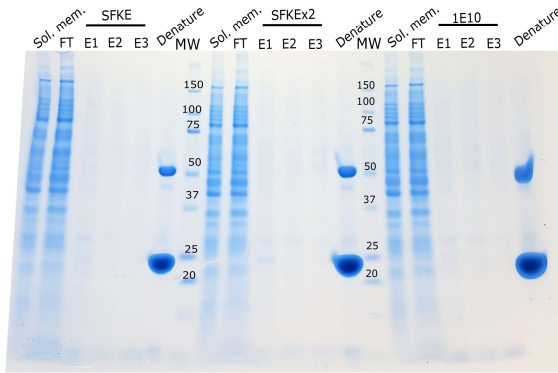


Figure 4.5A: Multivalent 1D4 peptide for improved elution from 1D4 column. Bovine rhodopsin from ROS was solubilized in 1X PBSSC + 1% DDM, then purified using 1D4-coupled Sepharose. Elutions were performed by addition of either 200 μ M 1D4 peptide (TETSQVAPA) or 1D4x2 peptide (TETSQVAPAEETETSQVAPA). Gel was visualized with Instant Blue (Coomassie).

CB1 GL G88; 1E10 coupled beads



CB1 GL G88; 1E10 coupled beads

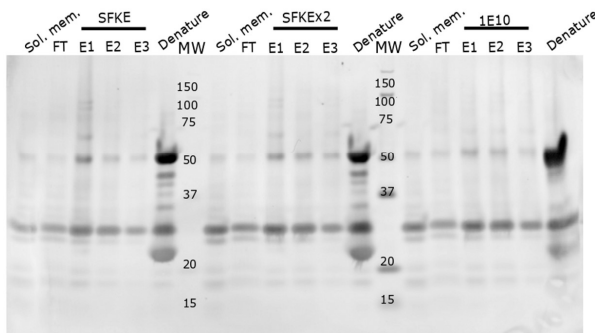


Figure 4.5B: Test of multivalent SFKE peptide for improving elution from 1E10 column. CB1-GL G88 was solubilized in 1X PBSSC + 1% DDM, then purified with 1E10-coupled Sepharose. Elutions were performed with 200 μ M SFKE peptide (SFKE), SFKEx2 peptide (SFKEGGGSFKE), or 1E10 peptide (SFKENEENIQ). Top gel is imaged with Instant Blue (Coomassie). Bottom western blot was stained with 1D4 primary antibody and goat-anti-mouse AF680 secondary.

4.6 Tables

Table 4.1: Peptides obtained from Genscript for use in protein purification.

Peptide	Sequence	Modification	Purity
SFKE	SFKE	N-terminal acetylation	>95%
1E10	SFKENEENIQ	N-terminal acetylation	>95%
1D4	TETSQVAPA	None	>99%
SFKEx2	SFKEGGGGSFKE	N-terminal acetylation	>85%
1D4x2	TETSQVAPAEETETSQVAPA	None	>85%

Chapter 5: Summary and Future Directions

5.1: Summary of significance

G-protein coupled receptors (GPCRs) are a family of transmembrane proteins that transduce signals across a membrane. Approximately 30-40% of all FDA approved drugs target a GPCR⁵. One of these receptors, the cannabinoid type 1 receptor (CB1) is a class A GPCR that interacts with endogenous ligands N-arachidonylethanolamine (Anandamide) and 2-Arachidonoylglycerol (2-AG)⁹⁻¹¹, phytocannabinoids like Δ^9 THC⁸, and synthetic agonists such as CP-55940 and Win 55212-2⁷⁰. CB1 is located throughout the central nervous system and plays a role in synaptic plasticity^{20,26,71-73}. Despite the important role CB1 plays in both normal physiologic activities and in disease states such as Parkinson's disease, Alzheimer's disease, multiple sclerosis, epilepsy, depression and more^{12,13}, new tools to examine the structure and expression of this important receptor are still needed.

One intriguing aspect about CB1 is that it retains such an unusually long N-terminus for a class A GPCR, and this region currently has no well-defined function. Previous analysis of CB1 mutants has shown that the majority of the CB1 N-terminus can be deleted without blocking receptor signaling, however, several cysteine residues in the N-terminus can modulate receptor activity³⁵. Given the length and conservation of this region, it is very possible that it is involved in an additional role in receptor modulation. There is increasing evidence for a potential role of an intracellular population of CB1 that can signal, and the CB1 N-terminus may play a role in this localization²⁹⁻³¹. It remains unclear how CB1 is distributed and how the subcellular localization of CB1 is modulated.

This thesis begins to address these gaps in knowledge by characterizing and validating three novel anti-CB1 monoclonal antibodies, and by generating and validating two N-terminal tags for use with one of these antibodies, 1E10. Furthermore, several applications of these antibodies were explored specifically to study the role of post- or co-translational modification on subcellular localization of CB1. Finally, this thesis explores the functionality of the N-terminal antibody, 1E10, in immunoaffinity

purification and attempts to improve classic immunoaffinity purification with multiplexed antibody epitopes.

5.2: Characterization and validation of novel anti-CB1 antibodies and generation of a novel visualization tag.

Novel anti-CB1 monoclonal antibodies generated for the Farrens lab by Dr. Dan Crawley (OHSU VGTI) and Dr. Jon Fay (OHSU, Farrens lab) were initially characterized by Dr. Jon Fay³⁷. I carried out a more extensive characterization of three of these antibodies, identifying the specific epitope of each antibody. Two of these antibodies, 5G3 and 3A3, share an epitope in the intracellular loop 3 region of CB1. Both of these antibodies were also validated for use in immunoblot, immunoprecipitation, and immunofluorescence.

The third monoclonal antibody, 1E10, was also characterized and validated. This antibody binds a short epitope located at the extreme N-terminus of the mutant the antibody was generated against, CB1_GL^{37,45}. Through a series of peptide competition assays and alanine scans, I identified four key residues that contribute the most to this antibody epitope – SFKE. One of these peptide competition immunoprecipitation assays strongly suggests that an N-terminal acetyl group is part of the antibody epitope. Moreover, a second peptide competition immunoprecipitation assay suggests that this acetylation must occur after the cleavage of the start methionine, as neither of the peptides containing a methionine (MSFKE) were able to compete with the 1E10 antibody binding. Together, these data reveal a short epitope beginning SFKE with a preference for an obligate acetylated N-terminus.

When added to another GPCR, rhodopsin, both 10- and 4-residue versions of the 1E10 epitope tag could be detected by the 1E10 antibody in immunoblots. Of note, the 4-residue tag disrupted the activation of rhodopsin less than the 10-residue tag, likely because it had less of an impact on receptor glycosylation. Further validation of these tags in other proteins, including soluble proteins, could

increase the impact of these tags. In particular, the 4-residue tag could be used with proteins that do not perform well with other N-terminal tags, such as the Flag tag.

5.3: Role of the CB1 N-terminus in CB1 subcellular localization.

To study the impact of the CB1 N-terminus on receptor localization in the cell, the novel anti-CB1 antibodies described above were used in conjunction with commercially available antibodies to visualize transiently transfected CB1 mutants. Transient transfection conditions were optimized for immunofluorescence in HEK 293 cells, then two labeling schemes were validated for use in exploring the role of the CB1 N-terminus in receptor subcellular expression. First, a labeling scheme was developed to visualize receptors using primary antibodies from the same species, allowing for multiplexed imaging of transiently expressed receptors. A second strategy was employed to visualize untagged, full-length receptor and perform a co-localization analysis to assess the potential for glycosylation and/or proteolytic cleavage of some or all the N-terminus to play a role in CB1 subcellular localization.

In all experiments, the use of transient expression resulted in a high degree of heterogeneity, which prevented meaningful analysis. Future studies would benefit from stable cell lines or endogenous sources. Neuronal cell lines, such as Neuro2a cells, could be a better system for future studies as they express wild type CB1⁷⁴. Using an endogenous expression system would be more physiologically relevant and would remove artifacts caused by overexpression. Several of the novel anti-CB1 antibodies, intracellular binding 3A3 and 5G3, recognize wild-type CB1 and could be used in this system to evaluate CB1 expression. Appropriate validation and controls would need to be conducted to validate these novel antibodies for use in this system.

5.4: Affinity-based purification strategies.

Preliminary data is promising for the use of 1E10 in immunoaffinity purification. 1E10 coupled sepharose could be used to purify several constructs including tagged rhodopsin mutants. There is still room for improvement, particularly in the elution of receptor. Reducing the affinity of the antibody for the tag by mutating the epitope improved elution from the 1E10 column for the single glycine addition mutant (CB1-GL G88), but not for the double alanine mutant (CB1-GL K90A, E91A). Detergent also had an impact on purification conditions. Purification with 1E10 coupled sepharose appeared to be improved with the use of RIPA buffer, while purifications with 1D4 coupled sepharose was improved with dodecylmaltoside (DDM). DDM is a commonly used detergent in GPCR studies as it is a gentle, non-ionic detergent that has been shown to work in functional assays of GPCRS ^{45,46,64}. RIPA buffer contains P-Nonidet, a non-ionic detergent, and deoxycholate, an ionic detergent. This makes it a poor candidate for functional studies of GPCRs. Overall, 1D4 outperforms 1E10 for immunoaffinity purification. This is likely because the affinity of 1D4 for its epitope is more moderate than 1E10, which enables better elution off the column using competing peptides. Consistent with this interpretation, immunoaffinity purification with 1E10 improved with addition of a glycine residue in front of the epitope region to reduce affinity for the epitope. In addition, 1D4 performs better in gentler detergent such as DDM, while 1E10 appears to prefer harsher detergent conditions as seen in RIPA.

Multiplexed peptides containing two antibody epitopes were used to attempt to improve elution from 1D4 and 1E10 columns. This concept has been employed previously with success with the anti-Flag antibody ⁷⁵. While there was a very slight improvement in elution from the 1D4 column in a preliminary test, there was no improvement in elution from the 1E10 column. The lack of overall success is likely attributable to the fact that both antibodies prefer an extreme end of the tagged protein. 1D4 works best when located at the extreme C-terminus and 1E10 works best when located at the extreme N-terminus. In order to take advantage of the increased local concentration provided by multiplexing,

branched peptides that maintain the end-preference of the antibody epitopes are more likely to be more successful than linear multiplexed peptides.

References:

1. Weis WI, Kobilka BK. The Molecular Basis of G Protein–Coupled Receptor Activation. *Annu Rev Biochem.* 2018;87:897-919. doi:10.1146/annurev-biochem-060614-033910
2. Tobin AB. G-protein-coupled receptor phosphorylation: where, when and by whom. *Br J Pharmacol.* 2008;153(Suppl 1):S167-S176. doi:10.1038/sj.bjp.0707662
3. Calebiro D, Godbole A. Internalization of G-protein-coupled receptors: Implication in receptor function, physiology and diseases. *Best Pract Res Clin Endocrinol Metab.* 2018;32(2):83-91. doi:10.1016/j.beem.2018.01.004
4. Yang D, Zhou Q, Labroska V, et al. G protein-coupled receptors: structure- and function-based drug discovery. *Signal Transduct Target Ther.* 2021;6(1):1-27. doi:10.1038/s41392-020-00435-w
5. Kooistra AJ, Mordalski S, Pándy-Szekeres G, et al. GPCRdb in 2021: integrating GPCR sequence, structure and function. *Nucleic Acids Res.* 2020;49(D1):D335-D343. doi:10.1093/nar/gkaa1080
6. Palczewski K, Kumasaka T, Hori T, et al. Crystal structure of rhodopsin: A G protein-coupled receptor. *Science.* 2000;289(5480):739-745. doi:10.1126/science.289.5480.739
7. Lagerström MC, Schiöth HB. Structural diversity of G protein-coupled receptors and significance for drug discovery. *Nat Rev Drug Discov.* 2008;7(4):339-357. doi:10.1038/nrd2518
8. Devane WA, Dysarz FA, Johnson MR, Melvin LS, Howlett AC. Determination and characterization of a cannabinoid receptor in rat brain. *Mol Pharmacol.* 1988;34(5):605-613.
9. Devane WA, Hanus L, Breuer A, et al. Isolation and structure of a brain constituent that binds to the cannabinoid receptor. *Science.* 1992;258(5090):1946-1949. doi:10.1126/science.1470919
10. Mechoulam R, Ben-Shabat S, Hanus L, et al. Identification of an endogenous 2-monoglyceride, present in canine gut, that binds to cannabinoid receptors. *Biochem Pharmacol.* 1995;50(1):83-90. doi:10.1016/0006-2952(95)00109-D
11. Sugiura T, Kondo S, Sukagawa A, et al. 2-Arachidonoylglycerol: A Possible Endogenous Cannabinoid Receptor Ligand in Brain. *Biochem Biophys Res Commun.* 1995;215(1):89-97. doi:10.1006/bbrc.1995.2437
12. Cristino L, Bisogno T, Di Marzo V. Cannabinoids and the expanded endocannabinoid system in neurological disorders. *Nat Rev Neurol.* 2020;16(1):9-29. doi:10.1038/s41582-019-0284-z
13. Hill MN, Miller GE, Vanessa Ho WS, Gorzalka BB, Hillard CJ. Serum Endocannabinoid Content is Altered in Females with Depressive Disorders: A Preliminary Report. *Pharmacopsychiatry.* 2008;41(2):48-53. doi:10.1055/s-2007-993211
14. Ryberg E, Vu HK, Larsson N, et al. Identification and characterisation of a novel splice variant of the human CB1 receptor. *FEBS Lett.* 2005;579(1):259-264. doi:10.1016/j.febslet.2004.11.085

15. Bagher AM, Laprairie RB, Kelly MEM, Denovan-Wright EM. Co-expression of the human cannabinoid receptor coding region splice variants (hCB1) affects the function of hCB1 receptor complexes. *Eur J Pharmacol.* 2013;721(1):341-354. doi:10.1016/j.ejphar.2013.09.002
16. Shire D, Carillon C, Kaghad M, et al. An Amino-terminal Variant of the Central Cannabinoid Receptor Resulting from Alternative Splicing (*). *J Biol Chem.* 1995;270(8):3726-3731. doi:10.1074/jbc.270.8.3726
17. Xiao JC, Jewell JP, Lin LS, Haggmann WK, Fong TM, Shen CP. Similar in vitro pharmacology of human cannabinoid CB1 receptor variants expressed in CHO cells. *Brain Res.* 2008;1238:36-43. doi:10.1016/j.brainres.2008.08.027
18. Andersson H, D'Antona AM, Kendall DA, Heijne GV, Chin CN. Membrane Assembly of the Cannabinoid Receptor 1: Impact of a Long N-Terminal Tail. *Mol Pharmacol.* 2003;64(3):570-577. doi:10.1124/mol.64.3.570
19. Degroot A, Köfalvi A, Wade MR, et al. CB1 Receptor Antagonism Increases Hippocampal Acetylcholine Release: Site and Mechanism of Action. *Mol Pharmacol.* 2006;70(4):1236-1245. doi:10.1124/mol.106.024661
20. Freund TF, Katona I, Piomelli D. Role of Endogenous Cannabinoids in Synaptic Signaling. *Physiol Rev.* 2003;83(3):1017-1066. doi:10.1152/physrev.00004.2003
21. Katona I, Sperlág B, Sík A, et al. Presynaptically Located CB1 Cannabinoid Receptors Regulate GABA Release from Axon Terminals of Specific Hippocampal Interneurons. *J Neurosci.* 1999;19(11):4544-4558. doi:10.1523/JNEUROSCI.19-11-04544.1999
22. Katona I, Urbán GM, Wallace M, et al. Molecular Composition of the Endocannabinoid System at Glutamatergic Synapses. *J Neurosci.* 2006;26(21):5628-5637. doi:10.1523/JNEUROSCI.0309-06.2006
23. Kawamura Y, Fukaya M, Maejima T, et al. The CB1 Cannabinoid Receptor Is the Major Cannabinoid Receptor at Excitatory Presynaptic Sites in the Hippocampus and Cerebellum. *J Neurosci.* 2006;26(11):2991-3001. doi:10.1523/JNEUROSCI.4872-05.2006
24. Nyíri G, Cserép C, Szabadits E, MacKie K, Freund TF. CB1 cannabinoid receptors are enriched in the perisynaptic annulus and on preterminal segments of hippocampal GABAergic axons. *Neuroscience.* 2005;136(3):811-822. doi:10.1016/j.neuroscience.2005.01.026
25. Oropeza VC, Mackie K, Van Bockstaele EJ. Cannabinoid receptors are localized to noradrenergic axon terminals in the rat frontal cortex. *Brain Res.* 2007;1127(1):36-44. doi:10.1016/j.brainres.2006.09.110
26. Twitchell W, Brown S, Mackie K. Cannabinoids Inhibit N- and P/Q-Type Calcium Channels in Cultured Rat Hippocampal Neurons. *J Neurophysiol.* 1997;78(1):43-50. doi:10.1152/jn.1997.78.1.43
27. Deadwyler SA, Hampson RE. Ensemble Activity and Behavior—What's the Code? *Science.* 1995;270(5240):1316-1316. doi:10.1126/science.270.5240.1316

28. Kendall DA, Yudowski GA. Cannabinoid Receptors in the Central Nervous System: Their Signaling and Roles in Disease. *Front Cell Neurosci.* 2017;10. doi:10.3389/fncel.2016.00294
29. Hebert-Chatelain E, Desprez T, Serrat R, et al. A cannabinoid link between mitochondria and memory. *Nature.* 2016;539(7630):555-559. doi:10.1038/nature20127
30. Bénard G, Massa F, Puente N, et al. Mitochondrial CB1 receptors regulate neuronal energy metabolism. *Nat Neurosci.* 2012;15(4):558-564. doi:10.1038/nn.3053
31. Hebert-Chatelain E, Reguero L, Puente N, et al. Cannabinoid control of brain bioenergetics: Exploring the subcellular localization of the CB1 receptor. *Mol Metab.* 2014;3(4):495-504. doi:10.1016/j.molmet.2014.03.007
32. Jakowiecki J, Abel R, Orzeł U, Pasznic P, Preissner R, Filipek S. Allosteric Modulation of the CB1 Cannabinoid Receptor by Cannabidiol—A Molecular Modeling Study of the N-Terminal Domain and the Allosteric-Orthosteric Coupling. *Molecules.* 2021;26(9):2456. doi:10.3390/molecules26092456
33. Hurst DP, Grossfield A, Lynch DL, et al. A Lipid Pathway for Ligand Binding Is Necessary for a Cannabinoid G Protein-coupled Receptor *. *J Biol Chem.* 2010;285(23):17954-17964. doi:10.1074/jbc.M109.041590
34. Reggio PH. Endocannabinoid Binding to the Cannabinoid Receptors: What Is Known and What Remains Unknown. *Curr Med Chem.* 2010;17(14):1468-1486.
35. Fay JF, Farrens DL. The membrane proximal region of the cannabinoid receptor CB1 N-terminus can allosterically modulate ligand affinity. *Biochemistry.* 2013;52(46):8286-8294. doi:10.1021/bi400842k
36. Esteban PF, Garcia-Ovejero D, Paniagua-Torija B, et al. Revisiting CB1 cannabinoid receptor detection and the exploration of its interacting partners. *J Neurosci Methods.* 2020;337:108680. doi:10.1016/j.jneumeth.2020.108680
37. Fay JF. *Purification and Structural Analysis of the Cannabinoid Receptor CB₁: Insights into Allosteric Regulation of a GPCR.* Oregon Health and Science University; 2012. <https://doi.org/10.6083/M4NG4NNF>
38. Fay JF, Dunham TD, Farrens DL. Cysteine Residues in the Human Cannabinoid Receptor: Only C257 and C264 Are Required for a Functional Receptor, and Steric Bulk at C386 Impairs Antagonist SR141716A Binding. *Biochemistry.* 2005;44(24):8757-8769. doi:10.1021/bi0472651
39. Shire D, Calandra B, Delpech M, et al. Structural Features of the Central Cannabinoid CB1 Receptor Involved in the Binding of the Specific CB1 Antagonist SR 141716A (*). *J Biol Chem.* 1996;271(12):6941-6946. doi:10.1074/jbc.271.12.6941
40. Song C, Howlett AC. Rat brain cannabinoid receptors are N-linked glycosylated proteins. *Life Sci.* 1995;56(23):1983-1989. doi:10.1016/0024-3205(95)00179-A
41. Ramesh K, Rosenbaum DM. Molecular basis for ligand modulation of the cannabinoid CB1 receptor. *Br J Pharmacol.* 2022;179(14):3487-3495. doi:10.1111/bph.15627

42. Moura LIF, Lemos C, Ledent C, Carvalho E, Köfalvi A. Chronic insulinopenia/hyperglycemia decreases cannabinoid CB1 receptor density and impairs glucose uptake in the mouse forebrain. *Brain Res Bull.* 2019;147:101-109. doi:10.1016/j.brainresbull.2019.01.024
43. Shen X, Duan H, Wang S, Hong W, Wang YY, Lin SL. Expression of Cannabinoid Receptors in Myometrium and its Correlation With Dysmenorrhea in Adenomyosis. *Reprod Sci.* 2019;26(12):1618-1625. doi:10.1177/1933719119833483
44. Lipman NS, Jackson LR, Trudel LJ, Weis-Garcia F. Monoclonal Versus Polyclonal Antibodies: Distinguishing Characteristics, Applications, and Information Resources. *ILAR J.* 2005;46(3):258-268. doi:10.1093/ilar.46.3.258
45. Fay JF, Farrens DL. A Key Agonist-induced Conformational Change in the Cannabinoid Receptor CB1 Is Blocked by the Allosteric Ligand Org 27569. *J Biol Chem.* 2012;287(40):33873-33882. doi:10.1074/jbc.M112.352328
46. Farrens DL, Dunham TD, Fay JF, Dews IC, Caldwell J, Nauert B. Design, expression, and characterization of a synthetic human cannabinoid receptor and cannabinoid receptor/ G-protein fusion protein. *J Pept Res Off J Am Pept Soc.* 2002;60(6):336-347. doi:10.1034/j.1399-3011.2002.21066.x
47. Heckman KL, Pease LR. Gene splicing and mutagenesis by PCR-driven overlap extension. *Nat Protoc.* 2007;2(4):924-932. doi:10.1038/nprot.2007.132
48. Fay JF, Farrens DL. Purification of Functional CB1 and Analysis by Site-Directed Fluorescence Labeling Methods. In: Reggio PH, ed. *Methods in Enzymology.* Vol 593. Cannabinoids and Their Receptors. Academic Press; 2017:343-370. doi:10.1016/bs.mie.2017.06.026
49. Kaushal S, Ridge KD, Khorana HG. Structure and function in rhodopsin: the role of asparagine-linked glycosylation. *Proc Natl Acad Sci U S A.* 1994;91(9):4024-4028.
50. Arnesen T, Van Damme P, Plevoda B, et al. Proteomics analyses reveal the evolutionary conservation and divergence of N-terminal acetyltransferases from yeast and humans. *Proc Natl Acad Sci.* 2009;106(20):8157-8162. doi:10.1073/pnas.0901931106
51. Wingfield P. N-Terminal Methionine Processing. *Curr Protoc Protein Sci.* 2017;88:6.14.1-6.14.3. doi:10.1002/cpp.29
52. Doi T, Molday RS, Khorana HG. Role of the intradiscal domain in rhodopsin assembly and function. *Proc Natl Acad Sci U S A.* 1990;87(13):4991-4995.
53. Franke RR, Sakmar TP, Oprian DD, Khorana HG. A single amino acid substitution in rhodopsin (lysine 248—leucine) prevents activation of transducin. *J Biol Chem.* 1988;263(5):2119-2122. doi:10.1016/S0021-9258(18)69178-1
54. Kaufman RJ. Identification of the components necessary for adenovirus translational control and their utilization in cDNA expression vectors. *Proc Natl Acad Sci.* 1985;82(3):689-693. doi:10.1073/pnas.82.3.689

55. Rio DC, Clark SG, Tjian R. A Mammalian Host-Vector System That Regulates Expression and Amplification of Transfected Genes by Temperature Induction. *Science*. 1985;227(4682):23-28. doi:10.1126/science.2981116
56. Yuan J, Xu WW, Jiang S, Yu H, Poon HF. The Scattered Twelve Tribes of HEK293. *Biomed Pharmacol J*. 2018;11(2):621-623.
57. Tan E, Chin CSH, Lim ZFS, Ng SK. HEK293 Cell Line as a Platform to Produce Recombinant Proteins and Viral Vectors. *Front Bioeng Biotechnol*. 2021;9:796991. doi:10.3389/fbioe.2021.796991
58. Beloborodov SS, Bao J, Krylova SM, Shala-Lawrence A, Johnson PE, Krylov SN. Aptamer facilitated purification of functional proteins. *J Chromatogr B*. 2018;1073:201-206. doi:10.1016/j.jchromb.2017.12.024
59. Gervais D. Quality Control and Downstream Processing of Therapeutic Enzymes. In: Labrou N, ed. *Therapeutic Enzymes: Function and Clinical Implications*. Springer; 2019:55-80. doi:10.1007/978-981-13-7709-9_3
60. Oliveira C, Domingues L. Guidelines to reach high-quality purified recombinant proteins. *Appl Microbiol Biotechnol*. 2018;102(1):81-92. doi:10.1007/s00253-017-8623-8
61. Labrou NE. Protein Purification Technologies. *Methods Mol Biol Clifton NJ*. 2021;2178:3-10. doi:10.1007/978-1-0716-0775-6_1
62. Taipa MÂ, Fernandes P, de Carvalho CCCR. Production and Purification of Therapeutic Enzymes. In: Labrou N, ed. *Therapeutic Enzymes: Function and Clinical Implications*. Springer; 2019:1-24. doi:10.1007/978-981-13-7709-9_1
63. Costa S, Almeida A, Castro A, Domingues L. Fusion tags for protein solubility, purification and immunogenicity in Escherichia coli: the novel Fh8 system. *Front Microbiol*. 2014;5:63. doi:10.3389/fmicb.2014.00063
64. Molday LL, Molday RS. 1D4 – A Versatile Epitope Tag for the Purification and Characterization of Expressed Membrane and Soluble Proteins. *Methods Mol Biol Clifton NJ*. 2014;1177:1-15. doi:10.1007/978-1-4939-1034-2_1
65. Hopp TP, Prickett KS, Price VL, et al. A Short Polypeptide Marker Sequence Useful for Recombinant Protein Identification and Purification. *Bio/Technology*. 1988;6(10):1204-1210. doi:10.1038/nbt1088-1204
66. Mammen M, Choi SK, Whitesides GM. Polyvalent Interactions in Biological Systems: Implications for Design and Use of Multivalent Ligands and Inhibitors. *Angew Chem Int Ed*. 1998;37(20):2754-2794. doi:10.1002/(SICI)1521-3773(19981102)37:20<2754::AID-ANIE2754>3.0.CO;2-3
67. Ueda M, Manabe Y, Mukai M. The high performance of 3XFLAG for target purification of a bioactive metabolite: A tag combined with a highly effective linker structure. *Bioorg Med Chem Lett*. 2011;21(5):1359-1362. doi:10.1016/j.bmcl.2011.01.038

68. Schafer CT, Shumate A, Farrens DL. Novel fluorescent GPCR biosensor detects retinal equilibrium binding to opsin and active G protein and arrestin signaling conformations. *J Biol Chem*. 2020;295(51):17486-17496. doi:10.1074/jbc.RA120.014631
69. Oprian DD, Molday RS, Kaufman RJ, Khorana HG. Expression of a synthetic bovine rhodopsin gene in monkey kidney cells. *Proc Natl Acad Sci*. 1987;84(24):8874-8878. doi:10.1073/pnas.84.24.8874
70. Slipetz DM, O'Neill GP, Favreau L, et al. Activation of the human peripheral cannabinoid receptor results in inhibition of adenylyl cyclase. *Mol Pharmacol*. 1995;48(2):352-361.
71. Herkenham M, Lynn AB, Johnson MR, Melvin LS, Costa B de, Rice KC. Characterization and localization of cannabinoid receptors in rat brain: a quantitative in vitro autoradiographic study. *J Neurosci*. 1991;11(2):563-583. doi:10.1523/JNEUROSCI.11-02-00563.1991
72. Leo LM, Abood ME. CB1 Cannabinoid Receptor Signaling and Biased Signaling. *Molecules*. 2021;26(17):5413. doi:10.3390/molecules26175413
73. Mackie K. Cannabinoid Receptors: Where They are and What They do. *J Neuroendocrinol*. 2008;20(s1):10-14. doi:10.1111/j.1365-2826.2008.01671.x
74. Graham ES, Ball N, Scotter EL, Narayan P, Dragunow M, Glass M. Induction of Krox-24 by Endogenous Cannabinoid Type 1 Receptors in Neuro2A Cells Is Mediated by the MEK-ERK MAPK Pathway and Is Suppressed by the Phosphatidylinositol 3-Kinase Pathway *. *J Biol Chem*. 2006;281(39):29085-29095. doi:10.1074/jbc.M602516200
75. Flag-tag and 3x Flag-tag | Proteintech. Accessed September 9, 2024. <https://www.ptglab.com/news/blog/flag-tag-and-3x-flag-tag/>
76. Grant GA, Crankshaw MW, Gorka J. [17] Edman sequencing as tool for characterization of synthetic peptides. In: *Methods in Enzymology*. Vol 289. Solid-Phase Peptide Synthesis. Academic Press; 1997:395-419. doi:10.1016/S0076-6879(97)89056-8
77. Komatsu S. Edman Sequencing of Proteins from 2D Gels. In: Thiellement H, Zivy M, Damerval C, Méchin V, eds. *Plant Proteomics: Methods and Protocols*. Humana Press; 2007:211-217. doi:10.1385/1-59745-227-0:211

Appendix 1: Primer list

Table A1: Primer list and primer properties.

Name	Sequence	length	GC %	TM (C)
CB1_IL3 del 1 FWD	CAGCCACGCCGTGCGGATGATCCAGCGGAGTGAGGACG GCAAG	43	67.4	77.1
CB1_IL3 del 2 FWD	CAGCCACGCCGTGCGGATGATCCAGCGGGGCACCCAGA AGAAGGTGCAAGTG	52	65.4	78.9
CB1_IL3 del 3 FWD	CAGCCACGCCGTGCGGATGATCCAGCGGGGCACCCAGA AGAGCATCATCATCCACACTGACCAGGCGCGG	70	65.7	81.9
CB1_NtRev	CGTGTGCAGGATCACGCACAGTAC	24	58.33	62.17
Rho_1E10_Fwd	CTGCAAGAATTCCACCATGTCTTCAAGGAGAACGAGGA GAACATCCAGAATGGCACAGAAGGC	64	50	73.6
Rho_1E10_Rev	CGAGCACTGCAGGCCCTCGGGATGTACTCTGGA	33	66.7	72.5
CB1_GL_I233A_H23 4A_fwd	GAAGAGCATCATCGCCGCCACCAAGTGAGGACG	32	62.5	69.8
CB1_GL_I233A_H23 4A_rev	CGTCCTCACTGGTGGCGGCGATGATGCTCTTC	32	62.5	69.8
CB1_GL_T235A_S23 6A_fwd	GCATCATCATCCACGCTGCTGAGGACGGCAAGG	33	60.6	69.9
CB1_GL_T235A_S23 6A_rev	CCTTGCCGTCCTCAGCAGCGTGGATGATGATGC	33	60.6	69.9
CB1_GL_E237A_D2 38A_fwd	CATCATCCACACCAAGTGCGGCCGCAAGGTGC	32	65.6	72.2
CB1_GL_E237A_D2 38A_rev	GCACCTTGCCGGCCGCACTGGTGTGGATGATG	32	65.6	72.2
CB1_GL_G239A_K2 40A_fwd	CATCCACACTAGCGAGGACGCCGCGGTGCAAGTG	34	64.7	72.3
CB1_GL_G239A_K2 40A_rev	CACTTGCACCGCGGCTCCTCGCTAGTGTGGATG	34	64.7	72.3
CB1_GL_V241A_Q2 42A_fwd	GAGGACGGCAAGGCGGCCGTGACCCGCC	28	78.6	74.8
CB1_GL_V241_Q24 2A_rev	GGCGGGTCACGGCCGCTTGCCGTCCTC	28	78.6	74.8
CB1_GL_V243A_T24 4A_fwd	GCAAGGTGCAAGCGGCGGCCCGACC	27	77.8	75
CB1_GL_V243A_T24 4A_rev	GGTCGGGGCGCGCCGCTTGCACCTTGC	27	77.8	75
CB1_GL_S2_insert_f wd	CCAAGTCAAGAATTCCACCATGTCTCCTTCAAGGAGAA CGAGG	45	51.1	69.8
CB1_GL_R2_insert_ fwd	CCAAGTCAAGAATTCCACCATGCGCTCCTTCAAGGAGA ACGAGG	45	53.3	71.4
CB1_GL_NT_mut_re v	GGTAGGTTTCATCGATGTGGGGGAAGATGTC	31	51.6	63.4
CB1_C2_1E10_inser t_fwd	GCAAGAATTCCACCATGTCTTCAAGGAGAACGAGGAGA ACATCCAGAAGTCCATCCTGGACGGC	65	52.3	74.4

CB1_GL_S2R_fwd_2	GGTCCAAGTCAAGAATTCCACCATGCGCTTCAAGGAGACG	42	52.4	70.4
CB1_GL_S88A_F89A_fwd	CTGCAAGAATTCCACCATGGCCGCAAGGAGAACG	35	57.1	69.7
CB1_GL_K90A_E91A_fwd	CTGCAAGAATTCCACCATGTCCTTCGCGGCGAACGAGGAG	40	57.5	71.6
CB1_GL_N92A_E93A_fwd	CTGCAAGAATTCCACCATGTCCTTCAAGGAGGCGCGGAGAACATCC	47	55.3	72.7
CB1_GL_E94A_N95A_fwd	CTGCAAGAATTCCACCATGTCCTTCAAGGAGAACGAGGCGCCATCCAGGCCG	53	58.5	75.7
CB1_GL_I96A_Q97A_fwd	CTGCAAGAATTCCACCATGTCCTTCAAGGAGAACGAGGAGAACGCCGCGGCCGCGGAG	58	60.3	77.5
CB1_GL_S88A_fwd	CTGCAAGAATTCCACCATGGCCTTCAAGGAGAACG	35	51.4	66.8
CB1_GL_F89A_fwd	CTGCAAGAATTCCACCATGTCCGCAAGGAGAACG	35	54.3	68.1
CB1_GL_K90A_fwd	CTGCAAGAATTCCACCATGTCCTTCGCGGAGAACGAGGAG	40	55	70
CB1_GL_E91A_fwd	CTGCAAGAATTCCACCATGTCCTTCAAGGCGAACGAGGAG	40	52.5	69.1
CB1_GL_G2_fwd	CCAAGTCAAGAATTCCACCATGGGCTCCTTCAAGGAG	38	52.6	68.4
pmt4_866_fwd	CGAGGAGGATTTGATATTCACCTGGCC	27	51.9	60.8
CB1_C2_1G88_fwd	CAAGAGCTTGAGCGGCTCCTTCAAGGAG	28	57.1	64.5
CB1_C2_1G88_rev	CTCCTTGAAGGAGCCGCTCAAGCTTTG	28	57.1	64.5
CB1_C2_4G88_fwd	CAAGAGCTTGAGCGGCGGCGGCTCCTTCAAGGAG	37	67.6	75.1
CB1_C2_4G88_rev	CTCCTTGAAGGAGCCGCCGCCGCTCAAGCTTTG	37	67.6	75.1
pmt4_1D4_rev	GGAATTTGCGGCCGCTTATGCAG	23	56.5	61.6
Rho_1E10_short_fwd	CTGCAAGAATTCCACCATGTCCTTCAAGGAGAACGAGAACG	46	50	70.2

Appendix 2: Edman sequencing of proteolytic product of CB1

Background:

The apparent molecular weight of CB1 varies depending on the experimental conditions^{36,42,43}. Additionally, there are often multiple bands on Western blots and the appearance of these bands can alter depending on the antibody used. Throughout work in the Farrens lab, a consistent band at ~40 kDa appears in addition to expected, slightly higher molecular weight bands in western blots of full-length CB1. To determine if this band represents a proteolytic product and if so, where the proteolysis occurs, Dr. Emily Platt submitted this band for Edman sequencing through the UC Davis proteomics center. Edman sequencing can analyze a protein or peptide sequence, beginning from the N-terminus⁷⁶. It generally requires that the N-terminus has been unmodified, or requires de-blocking steps⁷⁷.

Methods:

The construct used for this experiment was CB1-NtG9, which contains the intact CB1 Nt with GFP at the C-terminal tail after residue 417. In the analysis, ~7.5 ug of purified receptor in SMA nanodiscs were run on an 8% polyacrylamide gel, electro-transferred to PVDF membranes, and Coomassie stained (Figure A2). The band representing the lower molecular weight species (~40-45 kDa, arrowheads) was excised and submitted to the UC Davis proteomics center for Edman sequencing.

Results and discussion:

Edman sequencing returned the sequence SFKENE, which corresponds to residues 88-93 of the CB1 N-terminus, suggesting it was created by an 87-residue truncation of the N-terminus of CB1. Of note, this same region was omitted when creating the CB1-GL mutant, to increase solubility and expression of the receptor in mammalian expression systems^{37,38}. Purified CB1-GL was used to generate the antibodies described in this thesis, and the SFKENE sequence is the beginning of the epitope for the

1E10 antibody. Interestingly, 1E10 staining does not detect this band on western blots. Given that the 1E10 epitope contains an N-terminal acetyl group (see Chapter 2), it is likely that this proteolytic product is not N-terminally acetylated. This is reinforced by the technique itself, which is inhibited by N-terminal modification or blocking⁷⁷.

Figure:

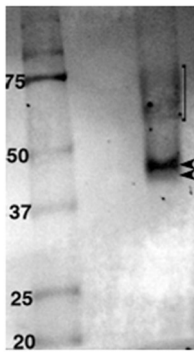


Figure A2: Coomassie stained PVDF membrane from SDS-PAGE of CB1-NtG9. Arrowheads indicate bands excised for Edman sequencing. Bracket indicates smear consistent with glycosylated full-length CB1.

Appendix 3: Live cell confocal microscopy of glycosylation-deficient mutant CB1

Background:

N-linked glycosylation has been previously described, but the role of this glycosylation remains unclear^{39,40}. The role of two potential sites of N-linked glycosylation in the CB1 N-terminus, N77 and N83, were tested by Dr. Emily Platt, who created a CB1 mutant with both asparagine residues mutated to glutamine to prevent N-linked glycosylation at these sites (N77Q, and N83Q). The parent construct used was a previously described synthetic human, full-length, minimal cysteine mutant, shCB1-C2³⁸.

Results and discussion:

Full-length CB1 (shCB1-C2) and glycosylation-deficient CB1 (N77Q/N83Q) were expressed in HEK 293S GNTI- cells and live cells were stained with an N-terminal polyclonal antibody recognizing the first 77 residues of the CB1 N-terminus followed by incubation with a goat anti-rabbit AF594 secondary antibody (Figure A3A). When applied to intact cells, this antibody will only be able to recognize surface expressed receptors. In the confocal images, the glycosylation deficient mutants appeared to show less labeling than the wild-type receptors, indicating that there was lower expression of the mutant at the plasma membrane. The expression of each construct was verified by western blot (Figure A3B). This western used 5G3, an intracellularly binding antibody characterized and validated in chapter 2. Given the total expression of the constructs were similar, the difference in surface staining suggests a connection between N-terminal, N-linked glycosylation and surface expression of CB1.

Figure:

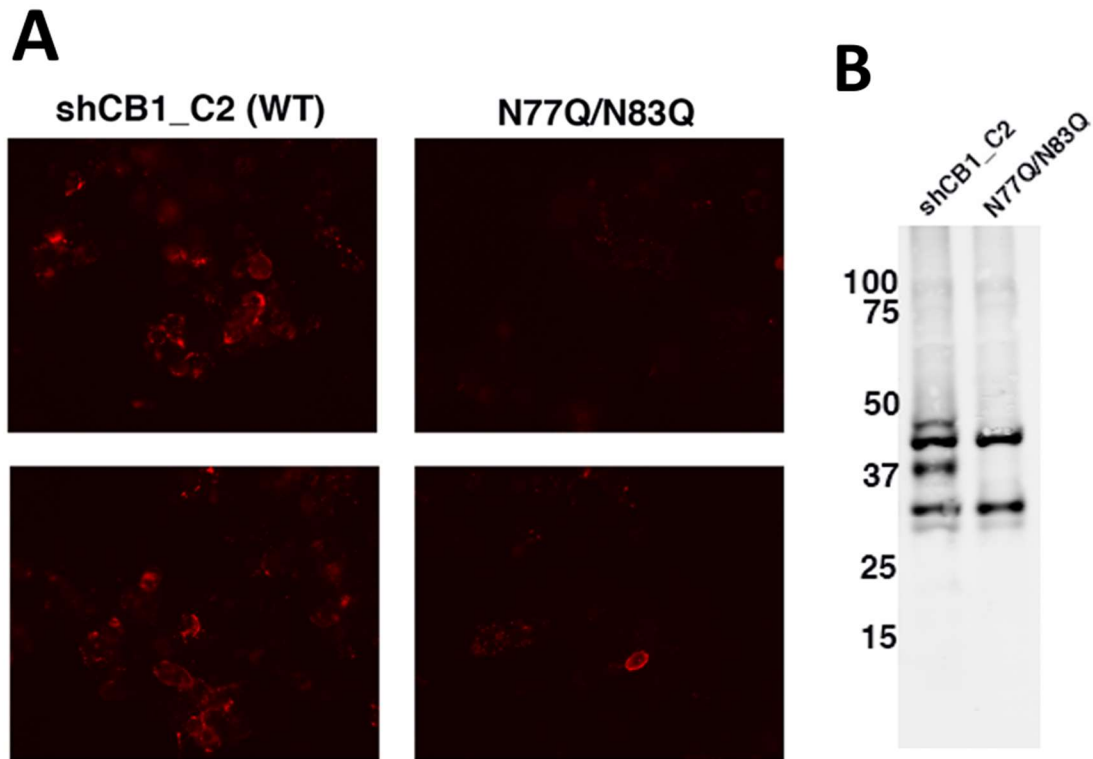


Figure A3: Immunofluorescence and western blot of shCB1-C2 or shCB1-C2 N77Q/N83Q in HEK 293

GNTI-. **A)** shCB1-C2 or shCB1-C2 N77Q/N83Q were transiently transfected into HEK 293 GNTI- cells. Live cells were stained with a rabbit anti-CB1 N-terminal (1-77) polyclonal antibody. **B)** Western blot of duplicate transfection of shCB1-C2 and shCB1-C2 N77Q/N83Q, visualized with 5G3.